40. Shimoike T, McKenna SA, Lindhout DA, Puglisi JD (2009) Translational insensitivity to potent activation of PKR by HCV IRES RNA. Antiviral Res 83: 228–237.
41. Nallagatla SR, Hwang J, Toroney R, Zheng X, Cameron CE, et al. (2007) 5′-triphosphate-dependent activation of PKR by RNAs with short stem-loops. Science 318: 1455–1458.
42. Gil J, Garcia MA, Gomez-Puertas P, Guerra S, Rullas J, et al. (2004) TRAF family proteins link PKR with NF-kappa B activation. Mol Cell Biol 24: 4502–4512.
43. Oganesyan G, Saha SK, Guo B, He JQ, Shahangian A, et al. (2006) Critical role of TRAF3 in the Toll-like receptor-dependent and -independent antiviral response. Nature 439: 208–211.
44. Zhang P, Samuel CE (2008) Induction of protein kinase PKR-dependent activation of interferon regulatory factor 3 by vaccinia virus occurs through adapter IPS-1 signaling. J Biol Chem 283: 34580–34587.
45. McAllister CS, Samuel CE (2009) The RNA-activated protein kinase enhances the induction of interferon-beta and apoptosis mediated by cytoplasmic RNA sensors. J Biol Chem 284: 1644–1651.
46. McAllister CS, Toth AM, Zhang P, Devaux P, Cattaneo R, et al. (2010) Mechanisms of protein kinase PKR-mediated amplification of beta interferon induction by C protein-deficient measles virus. J Virol 84: 380–386.
47. Strahle L, Marq JB, Brini A, Hausmann S, Kolakofsky D, et al. (2007) Activation of the beta interferon promoter by unnatural Sendai virus infection requires RIG-I and is inhibited by viral C proteins. J Virol 81: 12227–12237.
48. Biron-Andreani C, Raulet E, Pichard-Garcia L, Maurel P (2010) Use of human hepatocytes to investigate blood coagulation factor. Methods Mol Biol 640: 431–445.
49. Strahle L, Garcin D, Kolakofsky D (2006) Sendai virus defective-interfering genomes and the activation of interferon-beta. Virology 351: 101–111.
50. Jammi NV, Whitby LR, Beal PA (2003) Small molecule inhibitors of the RNA-dependent protein kinase. Biochem Biophys Res Commun 308: 50–57.
51. Nekhai S, Bottaro DP, Woldehawariat G, Spellerberg A, Petryshyn R (2000) A cell-permeable peptide inhibits activation of PKR and enhances cell proliferation. Peptides 21: 1449–1456.
52. Grandvaux N, Servant MJ, tenOever B, Sen GC, Balachandran S, et al. (2002) Transcriptional profiling of interferon regulatory factor 3 target genes: direct involvement in the regulation of interferon-stimulated genes. J Virol 76: 5532–5539.
53. Bonnet MC, Daurat C, Ottone C, Meurs EF (2006) The N-terminus of PKR is responsible for the activation of the NF-kappaB signaling pathway by interacting with the IKK complex. Cell Signal 18: 1865–1875.
54. Malakhov MP, Kim KI, Malakhova OA, Jacobs BS, Borden EC, et al. (2003) High-throughput immunoblotting. Ubiquitiin-like protein ISG15 modifies key regulators of signal transduction. J Biol Chem 278: 16608–16613.
55. Laurent AG, Krust B, Galabru J, Svab J, Hovanessian AG (1985) Monoclonal antibodies to interferon induced 68,000 Mr protein and their use for the detection of double-stranded RNA dependent protein kinase in human cells. Proc Natl Acad SciUSA 82: 4341–4345.
56. Iwano S, Ichikawa M, Takizawa S, Hashimoto H, Miyamoto Y (2010) Identification of AhR-regulated genes involved in PAH-induced immunotoxicity using a highly-sensitive DNA chip, 3D-Gene Human Immunity and Metabolic Syndrome 9k. Toxicol In Vitro 24: 85–91.
57. Wolff B, Sanglier JJ, Wang Y (1997) Leptomycin B is an inhibitor of nuclear export: inhibition of nucleo-cytoplasmic translocation of the human immunodeficiency virus type 1 (HIV-1) Rev protein and Rev-dependent mRNA. Chem Biol 4: 139–147.

Journal of General Virology (2011), 92, 2082–2087 DOI 10.1099/vir.0.032391-0

Short Communication

Structural requirements of virion-associated cholesterol for infectivity, buoyant density and apolipoprotein association of hepatitis C virus

Mami Yamamoto,[1,2] Hideki Aizaki,[1] Masayoshi Fukasawa,[3] Tohru Teraoka,[2] Tatsuo Miyamura,[1] Takaji Wakita[1] and Tetsuro Suzuki[1,4]

Correspondence
Tetsuro Suzuki
tesuzuki@hama-med.ac.jp

[1]Department of Virology II, National Institute of Infectious Diseases, Toyama 1-23-1, Shinjuku-ku, Tokyo 162-8640, Japan

[2]United Graduate School of Agricultural Science, Tokyo University of Agriculture and Technology, Saiwai-cho 3-5-8, Fuchu, Tokyo 183-8509, Japan

[3]Department of Biochemistry and Cell Biology, National Institute of Infectious Diseases, Toyama 1-23-1, Shinjuku-ku, Tokyo 162-8640, Japan

[4]Department of Infectious Diseases, Hamamatsu University School of Medicine, Handayama 1-20-1, Higashi-ku, Hamamatsu 431-3192, Japan

Received 22 March 2011
Accepted 17 May 2011

Our earlier study has demonstrated that hepatitis C virus (HCV)-associated cholesterol plays a key role in virus infectivity. In this study, the structural requirement of sterols for infectivity, buoyant density and apolipoprotein association of HCV was investigated further. We removed cholesterol from virions with methyl β-cyclodextrin, followed by replenishment with 10 exogenous cholesterol analogues. Among the sterols tested, dihydrocholesterol and coprostanol maintained the buoyant density of HCV and its infectivity, and 7-dehydrocholesterol restored the physical appearance of HCV, but suppressed its infectivity. Other sterol variants with a 3β-hydroxyl group or with an aliphatic side chain did not restore density or infectivity. We also provide evidence that virion-associated cholesterol contributes to the interaction between HCV particles and apolipoprotein E. The molecular basis for the effects of different sterols on HCV infectivity is discussed.

Hepatitis C virus (HCV) is a major cause of liver diseases, and is an enveloped, plus-strand RNA virus of the genus *Hepacivirus* of the family *Flaviviridae*. The mature HCV virion is considered to consist of a nucleocapsid, an outer envelope composed of the viral E1 and E2 proteins and a lipid membrane. Production and infection of several enveloped viruses, such as human immunodeficiency virus type 1 (HIV-1), hepatitis B virus and varicella-zoster virus (Bremer *et al.*, 2009; Campbell *et al.*, 2001; Graham *et al.*, 2003; Hambleton *et al.*, 2007), are dependent on cholesterol associated with virions. However, except for HIV-1 (Campbell *et al.*, 2002, 2004), there is limited information about the effects of replacing cholesterol with sterol analogues on the virus life cycle. We demonstrated the higher cholesterol content of HCV particles compared with host-cell membranes, and that HCV-associated cholesterol plays a key role in virion maturation and infectivity (Aizaki *et al.*, 2008). Recently, by using mass spectrometry, Merz *et al.* (2011) identified cholesteryl esters, cholesterol, phosphatidylcholine and sphingomyelin as major lipids of purified HCV particles.

To investigate further the effect of the structural requirement for cholesterol on the infectivity, buoyant density and apolipoprotein association of HCV, depletion of virion-associated cholesterol and substitution of endogenous cholesterol with structural analogues (Fig. 1a) was used in this study. HCVcc (HCV grown in cell culture) of the JFH-1 isolate (Wakita *et al.*, 2005), prepared as described previously (Aizaki *et al.*, 2008), was treated with 1 mM methyl β-cyclodextrin (B-CD), which extracts cholesterol from biological membranes, for 1 h at 37 °C. The cholesterol-depleted virus was then incubated with exogenous cholesterol or cholesterol analogues at various concentrations for 1 h. After removal of B-CD and free sterols by centrifugation at 38 000 r.p.m. (178 000 ***g***) for 2.5 h, the treated particles were used to infect Huh7 cells, kindly provided by Dr Francis V. Chisari (The Scripps Research Institute, La Jolla, CA, USA), and their infectivity was determined by quantifying the viral core protein in cells using an enzyme immunoassay (Ortho-Clinical Diagnostics) at 3 days post-infection (p.i.). Virus infectivity, which fell to <20 % after B-CD treatment, was

A supplementary table and figure are available with the online version of this paper.

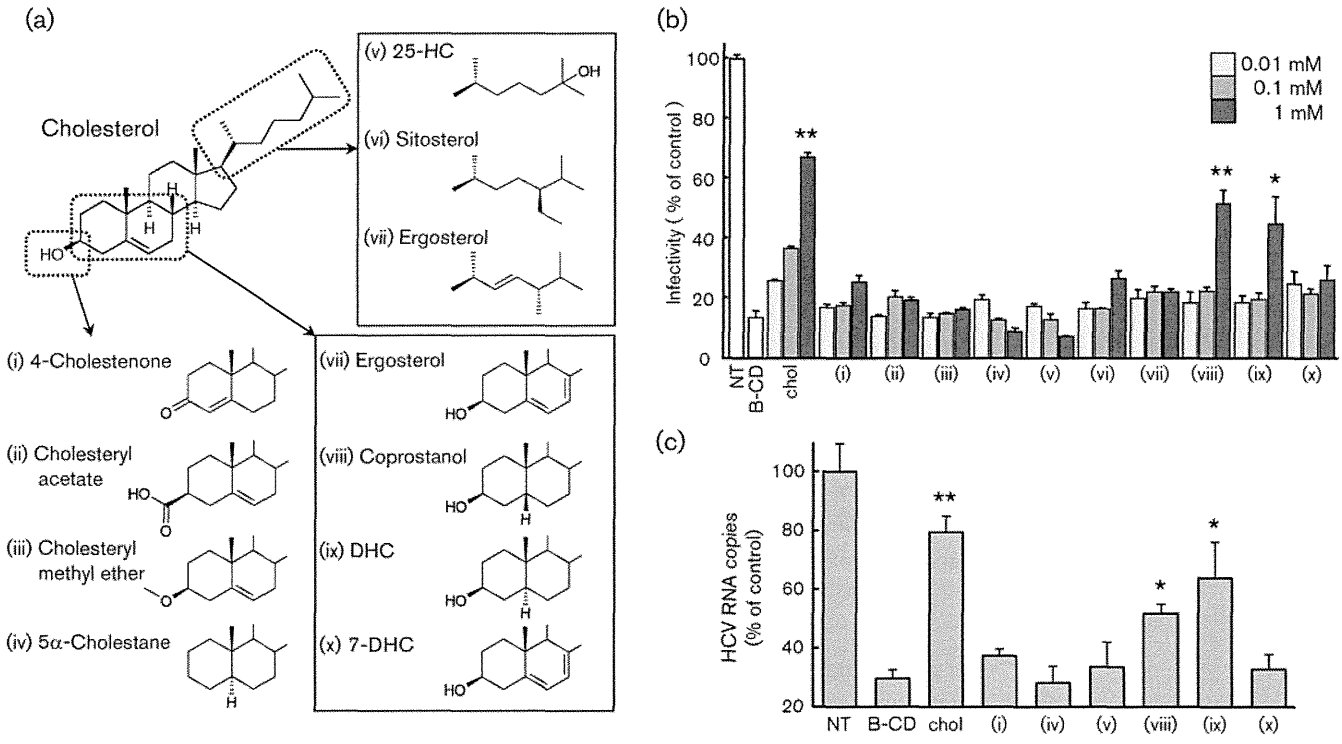

Fig. 1. Role of virion-associated cholesterol analogues in virus infection. (a) Structures of sterols used in this study. Variations in the 3β-hydroxyl group (lower left), aliphatic side chain (upper right) or ring structure (lower right) of cholesterol are shown. (i–x) Compounds studied in (b) and (c). (b) Effect of replenishment with sterols on HCV infectivity. Intracellular HCV core levels were determined at 72 h p.i. as the indicator of infectivity, which is represented as a percentage of the untreated HCVcc level (NT). (c) Effects of virion-associated sterols on virus internalization. HCV RNA copies in cells after virus internalization were quantified and are shown as percentages of the untreated HCVcc level (NT). (b, c) Means+SD of four samples are shown. *P<0.05; **P<0.01, compared with B-CD-treated virus (unpaired Student's t-test). Data are representative of at least two experiments.

recovered by addition of cholesterol at 0.01–1 mM in a dose-dependent manner (Fig. 1b). Among the cholesterol analogues tested, variants with a 3β-hydroxyl group (4-cholestenone, cholesteryl acetate, cholesteryl methyl ether and 5α-cholestane) or variants with an aliphatic side chain [25-hydroxycholesterol (25-HC), sitosterol and ergosterol] exhibited no or little effect on the recovery of infectivity of B-CD-treated HCV (Fig. 1b, lanes i–vii). In contrast, addition of variants in the structure of the sterol rings [coprostanol or dihydrocholesterol (DHC)] at 1 mM restored infectivity to around 50 % compared with non-treated virus control (Fig. 1b, lanes viii and ix). Other variants in the ring structure [7-dehydrocholesterol (7-DHC) and ergosterol, which is also a variant with an aliphatic side chain as indicated above] did not show any increase in the infectivity of B-CD-treated virus (Fig. 1b, lanes x and vii).

We demonstrated previously that HCV-associated cholesterol plays an important role in the internalization step of the virus, but not in cell attachment during virus entry (Aizaki *et al.*, 2008). The effect of virion-associated cholesterol analogues on virus attachment to cells and following internalization was determined. HCVcc, treated with B-CD with or without subsequent replenishment with sterols, was incubated with Huh7-25-CD81 cells, which stably express CD81 (Akazawa *et al.*, 2007), for 1 h at 4 °C. As an internalization assay, the incubation temperature was shifted to 37 °C post-binding procedure and maintained for 2 h. The cells were then treated with 0.25 % trypsin for 10 min at 37 °C, by which >90 % of HCV bound to the cell surface was removed (data not shown; Aizaki *et al.*, 2008). Internalized HCV was quantified by measuring the viral RNA in cell lysates by real-time RT-PCR (Takeuchi *et al.*, 1999). B-CD treatment or supplementation with sterols of B-CD-treated HCV had little or no effect on virus attachment to the cell surface (data not shown). Regarding virus internalization (Fig. 1c), treatment of HCVcc with 1 mM B-CD resulted in approximately 70 % reduction of viral RNA. The reduced level of the internalized HCV recovered markedly to approximately 80 % of the untreated HCVcc level by replenishment with 1 mM cholesterol. In agreement with the results shown in Fig. 1(b), addition of coprostanol or DHC to the B-CD-treated virus caused a significant recovery of virus internalization, suggesting that coprostanol and DHC associated with the

virion have the ability to play a role in HCV internalization into cells, in a manner comparable to cholesterol (Fig. 1c, lanes viii and ix). No or only a little recovery of virus internalization was observed by loading with other cholesterol analogues, such as 4-cholestenone, 5α-cholestane, 25-HC or 7-DHC (Fig. 1c, lanes i, iv, v and x).

To monitor the effect of cholesterol analogues on the physical characteristics of HCV, we next investigated buoyant-density profiles by using sucrose density-gradient centrifugation, in which untreated, B-CD-treated and sterol-replenished HCVcc were concentrated and layered onto continuous 10–60 % (w/v) sucrose density gradients, followed by centrifugation at 35 000 r.p.m. (151 000 *g*) for 14 h. Fractions were collected and analysed for the core protein. Fig. 2 shows that the virus density became higher after treatment with B-CD and that cholesterol-replenished virus shifted the density of B-CD-treated HCV to the non-treated level. Consistent with the result shown in Fig. 1(b), no effect on restoration of the buoyant densities of HCV was observed using variants with modifications in either the 3β-hydroxyl group (4-cholestenone, cholesteryl acetate and 5α-cholestane) or the aliphatic side chain (25-HC and sitosterol). In contrast, variants in the sterol ring structure (coprostanol, DHC and 7-DHC) had an ability to recover the density of B-CD-treated virus to that of non-treated virus.

Incorporation efficiency of the sterols into the cholesterol-depleted HCVcc was further determined by gas chromatography with flame ionization detection (see Supplementary Table S1, available in JGV Online). Under the experimental conditions used, exogenously supplied cholesterol after B-CD treatment was able to restore cholesterol content in HCVcc almost to initial levels. When 4-cholestenone, cholesteryl acetate, 25-HC, DHC or 7-DHC was added to B-CD-treated HCVcc, virion-associated sterol levels were 146, 157, 68, 96 or 73 %, respectively, of that of the non-treated control. The proportion of cholesterol analogues to the total sterols incorporated was ⩾30 % when 4-cholestenone, cholesteryl acetate, DHC or 7-DHC was used; however, the proportion in the case of 25-HC was only 3 %. It may be that the hydrophilic modification of the aliphatic side chain leads to poor association with HCVcc.

Collectively, exogenous variants with the 3β-hydroxyl group, such as 4-cholestenone and cholesteryl acetate, can be incorporated into B-CD-treated HCVcc, but resulted in no recovery of virus infectivity, indicating the importance of the 3β-hydroxyl group of cholesterol associated with the virus envelope in HCV infectivity. In contrast, two variants with modification in their sterol ring structures, coprostanol and DHC, have the ability to substitute for cholesterol. However, 7-DHC, another variant within the sterol ring, is incorporated readily into the depleted virion and restores the virus density, HCV replenished with 7-DHC is not infectious. These facts suggest that reduced forms of the sterol ring (coprostanol and DHC) in virion-associated cholesterol can be permitted for maintaining virus infectivity. However, a molecule with an additional double bond in the ring structure (7-DHC) seems to fail to exhibit infectivity, presumably because the change reduces structural flexibility in the

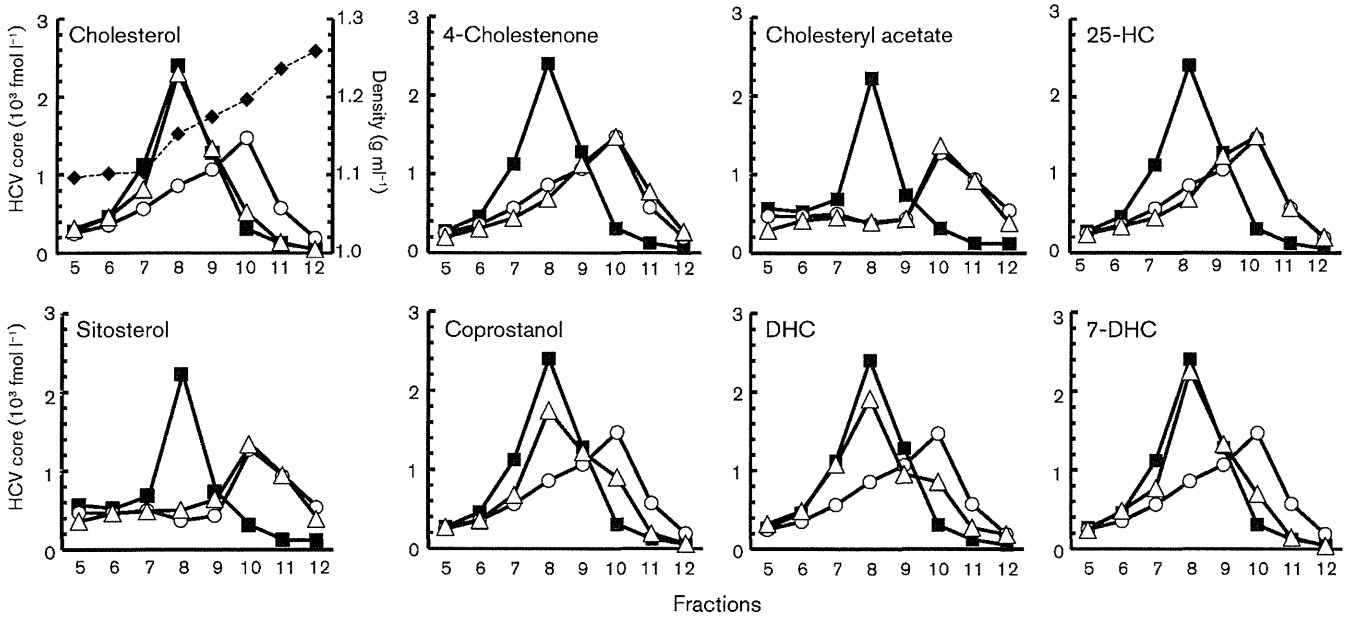

Fig. 2. Sucrose density-gradient profiles of lipid-modified HCV. Core protein concentration in each fraction of untreated HCVcc (■), B-CD-treated HCVcc (○) or HCVcc replenished with sterols (△) was determined. Corresponding densities of fractions are shown as a dashed line (◆).

sterol molecule and consequently in the virion structure. Coprostanol and DHC are *cis* and *trans* isomers, which are often known to have different physical properties. However, based on their molecular models, these two sterols, as well as cholesterol, possibly have similar spatial arrangements of the aliphatic side chain, the hydroxyl group and four-ring region because of their structural flexibility. In contrast, the spatial arrangement of 7-DHC does not seem comparable to that of cholesterol. Campbell *et al.* (2004) reported that replacement of HIV-1-associated cholesterol with raft-inhibiting sterols, including coprostanol, suppresses HIV-1 infectivity, whereas replacement with raft-promoting analogues such as DHC and 7-DHC (Megha *et al.*, 2006; Wang *et al.*, 2004; Xu & London, 2000; Xu *et al.*, 2001) maintains infectivity, demonstrating the importance of the raft-promoting properties of virion-associated cholesterol in HIV-1 infectivity (Campbell *et al.*, 2004). It is therefore likely that HCV-associated cholesterol is involved, at least in part, in virus infectivity via a molecular basis independent of lipid-raft formation.

The density of blood-circulating HCV is heterogeneous, ranging approximately from <1.06 to 1.25 g ml^{-1}, and it is proposed that low-density virus is associated with very-low-density lipoprotein (VLDL) and/or low-density lipoprotein (LDL) (André *et al.*, 2002; Thomssen *et al.*, 1993). It has recently been demonstrated that the pathway for VLDL assembly plays a role in assembly and maturation of infectious HCVcc (Icard *et al.*, 2009). HCVcc with low density, which is presumably associated with VLDL or VLDL-like lipoproteins, was found to possess higher infectivity than that with high density (Lindenbach *et al.*, 2006). This study, as well as our earlier work, indicated that removal of cholesterol from HCVcc by B-CD increased the buoyant density of the virus and reduced its infectivity. Thus, one may hypothesize that the virion-associated cholesterol plays a role in the formation of a complex with lipoproteins or apolipoproteins. To address this, the interaction between apolipoproteins and HCVcc with or without B-CD treatment was investigated by co-immunoprecipitation (Co-IP kit; Thermo Scientific). Virus samples were subjected separately to AminoLink Plus coupling resin, which was conjugated with a monoclonal antibody (mAb) against apolipoprotein E (ApoE) or apolipoprotein B (ApoB), and incubated at 4 °C for 4 h. After washing, total RNAs were extracted from the resulting resin beads by using TRIzol reagent (Invitrogen), followed by quantification of HCV RNA as described above (Takeuchi *et al.*, 1999). As indicated in Fig. 3(a), only a fraction of HCVcc was precipitated with an anti-ApoB mAb. In contrast, an anti-ApoE mAb was able to coprecipitate a considerable amount of the virus. It is of interest that B-CD-treated HCVcc hardly reacted with the mAb; however, the cholesterol-replenished virus was found to recover its reactivity, suggesting a role for virion-associated cholesterol in the formation of the HCV–lipoprotein/apolipoprotein complex. The results obtained are consistent with findings indicating that HCVcc can be captured with anti-ApoE antibodies, but capture with anti-ApoB antibodies is inefficient (Chang *et al.*, 2007; Hishiki *et al.*, 2010; Huang *et al.*, 2007; Jiang & Luo, 2009; Merz *et al.*, 2011; Nielsen *et al.*, 2006; Owen *et al.*, 2009), as well as with a recent model of structures of infectious HCV, in which HCVcc looks like ApoE-positive and primarily ApoB-negative lipoproteins (Bartenschlager *et al.*, 2011). We further tested the ApoE distribution in the density-gradient fractions of HCVcc samples (see Supplementary Fig. S1, available in JGV Online). With or without cholesterol depletion, ApoE was detected at a wide range of concentrations: 1.04 g ml^{-1} (fraction 1) to 1.17 g ml^{-1} (fraction 9). However, its level in the fractions at 1.10 g ml^{-1} (fraction 5) to approximately 1.17 g ml^{-1} was moderately decreased in the case of B-CD-treated virus.

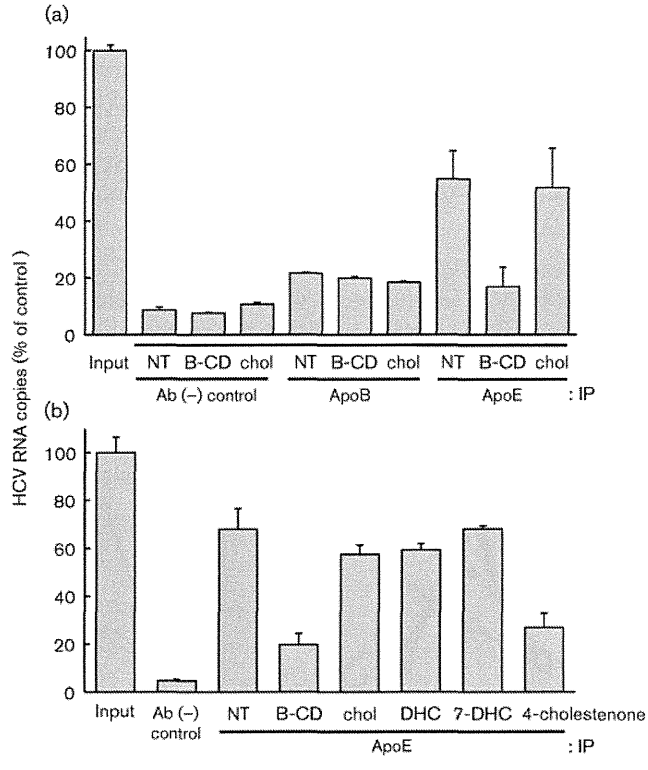

Fig. 3. Effect of virion-associated sterols on HCV–apolipoprotein interaction. (a) HCVcc samples with no treatment (NT), B-CD-treated (B-CD) or replenished with cholesterol (chol) were incubated with an amine-reactive resin coupling either an anti-ApoB mAb (ApoB) or an anti-ApoE mAb (ApoE). Control resin that is composed of the same material as above, but is not activated, was used as a negative control [Ab (–) control]. (b) B-CD-treated HCVcc was incubated with cholesterol (chol), DHC, 7-DHC or 4-cholestenone, followed by immunoprecipitation with the resin coupling with anti-ApoE mAb. (a, b) HCV RNAs in the immunoprecipitates were quantified and are indicated as percentages of the amount of input HCVcc RNA. Means+SD of three samples are shown. Data are representative of three experiments.

Whether cholesterol analogues could have a comparable role in HCV association with lipoprotein was examined further (Fig. 3b). Addition of DHC or 7-DHC, but not 4-cholestenone, to B-CD-treated HCVcc resulted in the recovery of coprecipitation of the virus with anti-ApoE. The results are correlated with the effect of sterols on the restoration of the buoyant densities of lipid-modified HCVcc (Fig. 2), suggesting that virion-associated cholesterol variants with modification in the sterol rings, but not in either the 3β-hydroxyl group or the aliphatic side chain, may tolerate the interaction between HCV and ApoE-positive lipoprotein.

Given that 7-DHC restored the association of HCV with ApoE and virion buoyant density, but did not restore infectivity, cholesterol and/or its analogues might affect the ability of virion membranes to fuse with the cell, independent of ApoE association. As cholesterol is an important mediator of membrane fluidity, one may hypothesize that HCV-associated cholesterol is involved in infectivity through modulation of the membrane fluidity. It has been reported that, in patients with Smith–Lemli–Opitz syndrome, a disorder of the cholesterol-synthesis pathway, cholesterol content decreases and 7-DHC increases in the cell membranes, leading to alteration of phospholipid packing in the membrane and abnormal membrane fluidity (Tulenko *et al.*, 2006).

It is now accepted that maturation and release of infectious HCV coincide with the pathway for producing VLDLs, which export cholesterol and triglyceride from hepatocytes. This study revealed roles for the structural basis of virion-associated cholesterol in the infectivity, buoyant density and apolipoprotein association of HCV. Although it was shown that HCV virions in infected patients, so-called lipo–viro particles, exhibited certain biochemical properties such as containing ApoB, ApoC and ApoE (Diaz *et al.*, 2006; Bartenschlager *et al.*, 2011), our studies provide useful information and the basis for future investigations toward a deeper understanding of the biogenesis pathway of infectious HCV particles.

Acknowledgements

We thank M. Matsuda, M. Sasaki and T. Date for technical assistance and T. Mizoguchi for secretarial work. This work was partially supported by a grant-in-aid for Scientific Research from the Japan Society for the Promotion of Science, from the Ministry of Health, Labor, and Welfare of Japan, and from the Ministry of Education, Culture, Sports, Science, and Technology.

References

Aizaki, H., Morikawa, K., Fukasawa, M., Hara, H., Inoue, Y., Tani, H., Saito, K., Nishijima, M., Hanada, K. & other authors (2008). Critical role of virion-associated cholesterol and sphingolipid in hepatitis C virus infection. *J Virol* **82**, 5715–5724.

Akazawa, D., Date, T., Morikawa, K., Murayama, A., Miyamoto, M., Kaga, M., Barth, H., Baumert, T. F., Dubuisson, J. & Wakita, T. (2007). CD81 expression is important for the permissiveness of Huh7 cell clones for heterogeneous hepatitis C virus infection. *J Virol* **81**, 5036–5045.

André, P., Komurian-Pradel, F., Deforges, S., Perret, M., Berland, J. L., Sodoyer, M., Pol, S., Bréchot, C., Paranhos-Baccalà, G. & Lotteau, V. (2002). Characterization of low- and very-low-density hepatitis C virus RNA-containing particles. *J Virol* **76**, 6919–6928.

Bartenschlager, R., Penin, F., Lohmann, V. & André, P. (2011). Assembly of infectious hepatitis C virus particles. *Trends Microbiol* **19**, 95–103.

Bremer, C. M., Bung, C., Kott, N., Hardt, M. & Glebe, D. (2009). Hepatitis B virus infection is dependent on cholesterol in the viral envelope. *Cell Microbiol* **11**, 249–260.

Campbell, S. M., Crowe, S. M. & Mak, J. (2001). Lipid rafts and HIV-1: from viral entry to assembly of progeny virions. *J Clin Virol* **22**, 217–227.

Campbell, S. M., Crowe, S. M. & Mak, J. (2002). Virion-associated cholesterol is critical for the maintenance of HIV-1 structure and infectivity. *AIDS* **16**, 2253–2261.

Campbell, S., Gaus, K., Bittman, R., Jessup, W., Crowe, S. & Mak, J. (2004). The raft-promoting property of virion-associated cholesterol, but not the presence of virion-associated Brij 98 rafts, is a determinant of human immunodeficiency virus type 1 infectivity. *J Virol* **78**, 10556–10565.

Chang, K. S., Jiang, J., Cai, Z. & Luo, G. (2007). Human apolipoprotein E is required for infectivity and production of hepatitis C virus in cell culture. *J Virol* **81**, 13783–13793.

Diaz, O., Delers, F., Maynard, M., Demignot, S., Zoulim, F., Chambaz, J., Trépo, C., Lotteau, V. & André, P. (2006). Preferential association of hepatitis C virus with apolipoprotein B48-containing lipoproteins. *J Gen Virol* **87**, 2983–2991.

Graham, D. R., Chertova, E., Hilburn, J. M., Arthur, L. O. & Hildreth, J. E. (2003). Cholesterol depletion of human immunodeficiency virus type 1 and simian immunodeficiency virus with β-cyclodextrin inactivates and permeabilizes the virions: evidence for virion-associated lipid rafts. *J Virol* **77**, 8237–8248.

Hambleton, S., Steinberg, S. P., Gershon, M. D. & Gershon, A. A. (2007). Cholesterol dependence of varicella-zoster virion entry into target cells. *J Virol* **81**, 7548–7558.

Hishiki, T., Shimizu, Y., Tobita, R., Sugiyama, K., Ogawa, K., Funami, K., Ohsaki, Y., Fujimoto, T., Takaku, H. & other authors (2010). Infectivity of hepatitis C virus is influenced by association with apolipoprotein E isoforms. *J Virol* **84**, 12048–12057.

Huang, H., Sun, F., Owen, D. M., Li, W., Chen, Y., Gale, M., Jr & Ye, J. (2007). Hepatitis C virus production by human hepatocytes dependent on assembly and secretion of very low-density lipoproteins. *Proc Natl Acad Sci U S A* **104**, 5848–5853.

Icard, V., Diaz, O., Scholtes, C., Perrin-Cocon, L., Ramière, C., Bartenschlager, R., Penin, F., Lotteau, V. & André, P. (2009). Secretion of hepatitis C virus envelope glycoproteins depends on assembly of apolipoprotein B positive lipoproteins. *PLoS One* **4**, e4233.

Jiang, J. & Luo, G. (2009). Apolipoprotein E but not B is required for the formation of infectious hepatitis C virus particles. *J Virol* **83**, 12680–12691.

Lindenbach, B. D., Meuleman, P., Ploss, A., Vanwolleghem, T., Syder, A. J., McKeating, J. A., Lanford, R. E., Feinstone, S. M., Major, M. E. & other authors (2006). Cell culture-grown hepatitis C virus is infectious *in vivo* and can be recultured *in vitro*. *Proc Natl Acad Sci U S A* **103**, 3805–3809.

Megha, Bakht, O. & London, E. (2006). Cholesterol precursors stabilize ordinary and ceramide-rich ordered lipid domains (lipid

rafts) to different degrees. Implications for the Bloch hypothesis and sterol biosynthesis disorders. *J Biol Chem* **281**, 21903–21913.

Merz, A., Long, G., Hiet, M. S., Brügger, B., Chlanda, P., Andre, P., Wieland, F., Krijnse-Locker, J. & Bartenschlager, R. (2011). Biochemical and morphological properties of hepatitis C virus particles and determination of their lipidome. *J Biol Chem* **286**, 3018–3032.

Nielsen, S. U., Bassendine, M. F., Burt, A. D., Martin, C., Pumeechockchai, W. & Toms, G. L. (2006). Association between hepatitis C virus and very-low-density lipoprotein (VLDL)/LDL analyzed in iodixanol density gradients. *J Virol* **80**, 2418–2428.

Owen, D. M., Huang, H., Ye, J. & Gale, M., Jr (2009). Apolipoprotein E on hepatitis C virion facilitates infection through interaction with low-density lipoprotein receptor. *Virology* **394**, 99–108.

Takeuchi, T., Katsume, A., Tanaka, T., Abe, A., Inoue, K., Tsukiyama-Kohara, K., Kawaguchi, R., Tanaka, S. & Kohara, M. (1999). Real-time detection system for quantification of hepatitis C virus genome. *Gastroenterology* **116**, 636–642.

Thomssen, R., Bonk, S. & Thiele, A. (1993). Density heterogeneities of hepatitis C virus in human sera due to the binding of beta-lipoproteins and immunoglobulins. *Med Microbiol Immunol (Berl)* **182**, 329–334.

Tulenko, T. N., Boeze-Battaglia, K., Mason, R. P., Tint, G. S., Steiner, R. D., Connor, W. E. & Labelle, E. F. (2006). A membrane defect in the pathogenesis of the Smith–Lemli–Opitz syndrome. *J Lipid Res* **47**, 134–143.

Wakita, T., Pietschmann, T., Kato, T., Date, T., Miyamoto, M., Zhao, Z., Murthy, K., Habermann, A., Kräusslich, H. G. & other authors (2005). Production of infectious hepatitis C virus in tissue culture from a cloned viral genome. *Nat Med* **11**, 791–796.

Wang, J., Megha & London, E. (2004). Relationship between sterol/steroid structure and participation in ordered lipid domains (lipid rafts): implications for lipid raft structure and function. *Biochemistry* **43**, 1010–1018.

Xu, X. & London, E. (2000). The effect of sterol structure on membrane lipid domains reveals how cholesterol can induce lipid domain formation. *Biochemistry* **39**, 843–849.

Xu, X., Bittman, R., Duportail, G., Heissler, D., Vilcheze, C. & London, E. (2001). Effect of the structure of natural sterols and sphingolipids on the formation of ordered sphingolipid/sterol domains (rafts). Comparison of cholesterol to plant, fungal, and disease-associated sterols and comparison of sphingomyelin, cerebrosides, and ceramide. *J Biol Chem* **276**, 33540–33546.

IJC
International Journal of Cancer

Inhibition of autophagy potentiates the antitumor effect of the multikinase inhibitor sorafenib in hepatocellular carcinoma

Satoshi Shimizu[1]*, Tetsuo Takehara[1]*, Hayato Hikita[1], Takahiro Kodama[1], Hinako Tsunematsu[1], Takuya Miyagi[1], Atsushi Hosui[1], Hisashi Ishida[1], Tomohide Tatsumi[1], Tatsuya Kanto[1], Naoki Hiramatsu[1], Naonobu Fujita[2], Tamotsu Yoshimori[2] and Norio Hayashi[3]

[1] Department of Gastroenterology and Hepatology, Osaka University Graduate School of Medicine, Suita, Osaka, Japan
[2] Department of Genetics, Osaka University Graduate School of Medicine, Suita, Osaka, Japan
[3] Kansai-Rosai Hospital, Amagasaki, Hyogo, Japan

Multikinase inhibitor sorafenib inhibits proliferation and angiogenesis of tumors by suppressing the Raf/MEK/ERK signaling pathway and VEGF receptor tyrosine kinase. It significantly prolongs median survival of patients with advanced hepatocellular carcinoma (HCC) but the response is disease-stabilizing and cytostatic rather than one of tumor regression. To examine the mechanisms underlying the relative resistance in HCC, we investigated the role of autophagy, an evolutionarily conserved self-digestion pathway, in hepatoma cells *in vitro* and *in vivo*. Sorafenib treatment led to accumulation of autophagosomes as evidenced by conversion from LC3-I to LC3-II observed by immunoblot in Huh7, HLF and PLC/PRF/5 cells. This induction was due to activation of autophagic flux, as there was further increase in LC3-II expression upon treatment with lysosomal inhibitors, clear decline of the autophagy substrate p62, and an mRFP-GFP-LC3 fluorescence change in sorafenib-treated hepatoma cells. Sorafenib inhibited the mammalian target of rapamycin complex 1 and its inhibition led to accumulation of LC3-II. Pharmacological inhibition of autophagic flux by chloroquine increased apoptosis and decreased cell viability in hepatoma cells. siRNA-mediated knockdown of the ATG7 gene also sensitized hepatoma cells to sorafenib. Finally, sorafenib induced autophagy in Huh7 xenograft tumors in nude mice and coadministration with chloroquine significantly suppressed tumor growth compared with sorafenib alone. In conclusion, sorafenib administration induced autophagosome formation and enhanced autophagic activity, which conferred a survival advantage to hepatoma cells. Concomitant inhibition of autophagy may be an attractive strategy for unlocking the antitumor potential of sorafenib in HCC.

Sorafenib is an orally available multikinase inhibitor recently approved as the first molecular targeting compound for hepatocellular carcinoma (HCC).[1] Sorafenib inhibits Raf kinases, including Raf-1 and B-Raf, which are members of the Raf/MEK/ERK signaling pathway, and inhibits a number of receptor tyrosine kinases involved in neo-angiogenesis and tumor progression, such as vascular endothelial growth factor receptor (VEGFR) 2, platelet-derived growth factor receptor β and c-Kit. Two randomized, placebo-controlled trials revealed that sorafenib significantly prolongs the median survival of patients with advanced HCC but the response is disease-stabilizing and cytostatic rather than one of tumor regression.[2,3] Therefore, a more detailed understanding of the mechanisms underlying both the antitumor effect and the primary resistance to this compound may provide insights that can help to improve the therapeutic outcome in HCC.

Macroautophagy (hereafter referred to as autophagy) is an evolutionally conserved catabolic process that transports cellular macromolecules and organelles to a lysosomal degradation pathway.[4] It is regulated by autophagy-related (*atg*) genes that control the formation and maturation of a double-membrane vesicle, autophagosome, which sequestrates cellular proteins and organelles. Autophagosomes then fuse with lysosomes to form autolysosomes, in which lysosomal enzymes digest the sequestered content and inner membrane. Autophagy is typically induced under starvation, initially considered to be a survival strategy that recycles cellular components to meet energy requirements. Autophagy also occurs at low basal levels in virtually all cells to perform homeostatic functions such as turnover of long-lived or damaged proteins and organelles. On the other hand, autophagy can mediate cell death under certain conditions probably through overactivation of self-digestion, which is considered to be Type II programmed cell death.[5] Therefore, autophagy can promote both cell survival and death depending on the cellular context and/or initiating stimulus.

Key words: liver, HCC, mTOR, tumor, apoptosis
Grant sponsors: Ministry of Education, Culture, Sports, Science and Technology, Japan; Ministry of Health, Labor and Welfare of Japan
*S.S. and T.T. contributed equally to this work and share first authorship.
DOI: 10.1002/ijc.26374
History: Received 4 Mar 2011; Accepted 3 Aug 2011; Online 19 Aug 2011
Correspondence to: Tetsuo Takehara, Department of Gastroenterology and Hepatology, Osaka University Graduate School of Medicine, 2-2 Yamada-oka, Suita, Osaka 565-0871, Japan, Tel.: +81-6-6879-3621, Fax: +81-6-6879-3629, E-mail: takehara@gh.med.osaka-u.ac.jp

Autophagy has been shown to be involved in cancer development and progression in a variety of ways.[6] Genetic evidence supports a tumor suppressive role of autophagy in cancer development. The *Beclin 1* autophagy gene is monoallelically deleted in a subset of human sporadic breast, ovarian and prostate cancer. Heterozygous disruption of *Beclin 1* increases the frequency of spontaneous malignancies in mice.[7] On the other hand, tumor cells display autophagy or autophagic cell death under a variety of stress-inducing conditions as well as anticancer therapies.[8] Therefore, autophagy promotes or inhibits tumor progression which is also dependent on the cell types and stimuli. Recently, sorafenib has been reported to induce autophagosome accumulation, as evidenced by GFP-LC3 markers, in tumor cells.[9–11] However, its biological and clinical significance has not yet been addressed. In the present study, we examined autophagy of hepatoma cells treated with sorafenib and demonstrate that sorafenib not only induces autophagosome formation but also activates autophagic flux which is an adaptive response to this compound, and that concomitant inhibition of autophagy may be therapeutically useful for improving the anti-HCC effect.

Material and Methods

Cell lines

Hepatoma cell lines Huh7, HLF and PLC/PRF/5 were cultured with Dulbecco's modified Eagle medium (DMEM). Huh7 and HLF were obtained from the JCRB/HSRRB cell bank (Osaka, Japan) and PLC/PRF/5 was obtained from ATCC (Manassas, VA). All cell lines were cultured at 37°C in a humidified atmosphere of 5% CO_2.

Western immunoblot

Cells or tissues were lysed and immunoblotted as previously described.[12] For immunodetection, the following antibodies were used: anti-microtubule-associated protein 1 light chain (LC3) polyclonal antibody (Ab) (MBL, Nagoya, Japan); anti-ATG7 polyclonal Ab (MBL); anti-Beclin1 polyclonal Ab (CST, Danvers, MA); anti-p62 polyclonal Ab (MBL); anti-phospho-ERK polyclonal Ab (CST); anti-phospho-S6K polyclonal Ab (CST); anti-phospho-4E-BP1 polyclonal Ab (CST); anti-phospho-Akt polyclonal Ab (CST).

Transfection with fluorescent LC3 plasmid

Cells were transfected with monomeric red fluorescence protein (mRFP)-GFP tandem fluorescent-tagged LC3 expression plasmid (ptfLC3)[13] using Fugene6 (Roche Applied Science, Hague Road, IN) according to the manufacturer's instructions. At 48 hr after transfection, the medium was changed to DMEM containing sorafenib or DMSO, and the cells were further cultured and examined under a BZ8100 fluorescent microscope (Keyence, Osaka, Japan).

In vitro treatment with sorafenib

Hepatoma cells were transfected with 5 nM Silencer Select siRNAs (Ambion, Austin, TX) either of *ATG7* or negative control using RNAiMAX (Invitrogen, Carlsbad, CA) according to the manufacturer's instructions. Forty-eight hours after transfection, the medium was changed to DMEM containing sorafenib or DMSO. Cells were further cultured and assayed for cell viability by WST assay using the cell count reagent SF (Nacalai Tesque, Kyoto, Japan) and analyzed for apoptosis using Annexin V-FITC apoptosis detection kit (Biovision, Mountain View, CA). We defined apoptotic cells as Annexin V-FITC positive and propidium iodide (PI) negative cells. PI negative cells were gated and the positive cell rate of Annexin V-FITC was determined. The supernatant of the cultured cells was assayed for caspase-3/7 activity using Caspase-Glo 3/7 assay (Promega, Madison, WI) as previously reported.[12] For the treatment with a pharmacological inhibitor of autophagy, cells were cultured with DMEM containing chloroquine (Sigma-Aldrich, St. Louis, MO) or bafilomycin A1 (Sigma-Aldrich) with sorafenib or DMSO and assayed for cell viability and caspase-3/7 activity in the same manner.

Electron microscopy

Samples were fixed with 2.5% glutaraldehyde solution buffered at pH 7.4 with 0.1 M Millonig's phosphate at 4°C for 2 hr, postfixed in 1% osmium tetroxide solution at 4°C for 1 hr, dehydrated in graded concentrations of ethanol and embedded in Nissin EM Quetol 812 epoxy resin. Ultrathin sections (80 nm) cut on a Reichert ultramicrotome (Ultracut E) were stained with uranyl acetate and lead citrate, and examined with a Hitachi H-7650 electron microscope at 80 kV.

Xenograft experiments

To produce a xenograft tumor, 3–5 $\times$ 10^6 Huh7 cells were subcutaneously injected to Balb/c nude mice. Sorafenib tablets were crushed and orally administered daily with water containing 12.5% cremophor EL (Sigma-Aldrich) and 12.5% ethanol, as previously described.[14] Chloroquine was dissolved in PBS and intraperitoneally administered daily. We estimated the volume of the xenograft tumor using the following formula: tumor volume = $\pi/6 \times$ (major axis) $\times$ (minor axis)^2. Mice were maintained in a specific pathogen-free facility and treated with humane care with approval from the Animal Care and Use Committee of Osaka University Medical School.

Statistical analysis

Data are presented as mean $\pm$ SD. Comparisons between two groups were performed by unpaired t test. Multiple comparisons were performed by ANOVA with Scheffe post-hoc test. $p < 0.05$ was considered statistically significant.

Results

In vitro treatment with sorafenib induces accumulation of autophagosomes in hepatoma cell lines

To examine the effect of sorafenib on autophagy in human HCC, we treated the hepatoma cell line Huh7 with sorafenib *in vitro*. First, we assessed the expression of LC3, a

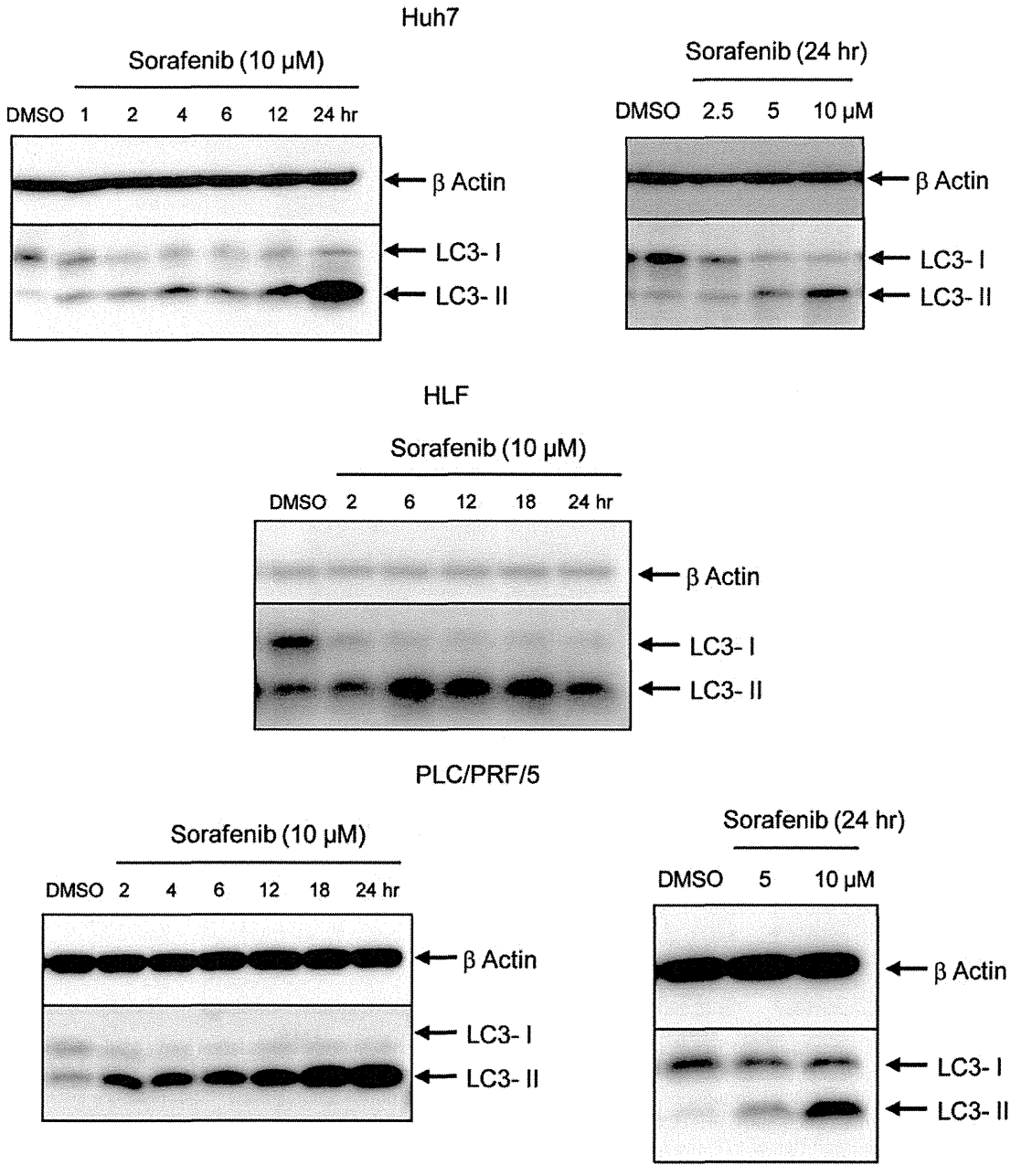

Figure 1. Sorafenib induces accumulation of autophagosomes in hepatoma cells. Western blot showing an increase in LC3-II in Huh7, HLF and PLC/PRF/5 hepatoma cells after treatment with sorafenib. Hepatoma cells were treated with 2.5, 5 or 10 μM sorafenib for the indicated times and analyzed for LC3 expression by western blot. Hepatoma cells treated with DMSO-containing media for 24 hr are shown as the control. [Color figure can be viewed in the online issue, which is available at wileyonlinelibrary.com.]

mammalian homolog of yeast *atg8*, by immunoblot. During the progress of autophagy, the cytoplasmic form LC3-I is converted to the membrane-bound lipidated form LC3-II which is detected by a mobility shift on electrophoresis.[15] When Huh7 cells were treated with 10 μM sorafenib, LC3 conversion was observed as early as 1 hr after the treatment and gradually increased at later time points (Fig. 1). We examined the dose-dependency of this response in Huh7 cells as well. Under 2.5 μM sorafenib treatment, the amount of LC3-II did not show an obvious increase, however, the amount of LC3-I decreased which indicates modest activation of autophagosome formation. Under 5 and 10 μM sorafenib treatment, the amount of LC3-II clearly increased. Next, we investigated the effect of sorafenib on other hepatoma cell lines, HLF and PLC/PRF/5. Under sorafenib treatment, LC3 conversion was observed at 2 hr after the initiation of treatment and gradually increased until 24 hr in HLF cells and PLC/PRF/5 cells in the same manner as in Huh7 cells.

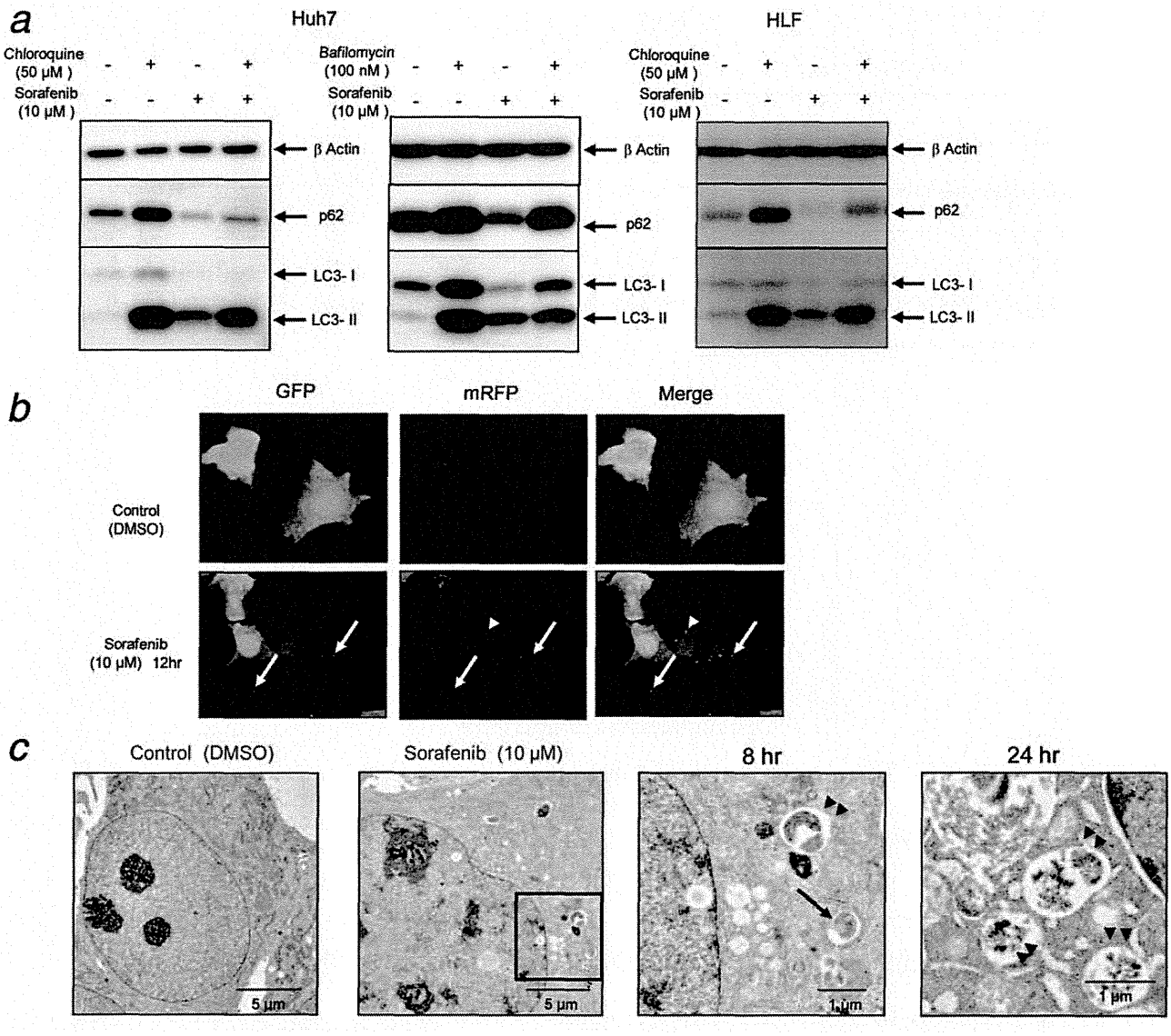

Figure 2. Sorafenib activates autophagic flux in hepatoma cells. (*a*). Western blot showing p62 degradation and LC3 lipidation in Huh7 cells and HLF cells treated with sorafenib and/or lysosomal inhibitors. Huh7 cells or HLF cells were treated with or without 10 μM sorafenib in the presence or absence of 50 μM chloroquine or 100 nM bafilomycin A1 for 12 hr. (*b*). Photographs of fluorescence microscopy of punctate fluorescence of a transfected mRFP-GFP-LC3 construct in Huh7 cells after 12-hr treatment with 10 μM sorafenib. Arrows indicate a typical example of colocalized particles of GFP and mRFP signal, while the arrowhead points to a typical example of a particle with an mRFP signal but without a GFP signal. *C.* Photographs from transmission electron microscopy showing autophagic vacuoles including autophagosomes (arrow) and probably autolysosomes (arrowhead) in Huh7 cells treated with 10 μM sorafenib.

Sorafenib activates autophagic flux in hepatoma cells

To clarify whether the accumulation of autophagosomes induced by sorafenib is a result of induction of autophagosome formation or inhibition of autophagosome degradation, we first measured the amount of p62, a selective substrate of autophagy, by immunoblot. Activation of the autophagic flux leads to a decline in p62 expression, and *vice versa*.[16] When Huh7 cells or HLF cells were treated with sorafenib, the amount of p62 decreased despite the accumulation of LC3-II implying that this accumulation of LC3-II is associated with autophagosome degradation (Fig. 2*a*). In addition, when cells were treated with both sorafenib and chloroquine, accumulation of LC3-II was further enhanced compared to the sorafenib-treated group, while the levels of p62 expression increased. We also used bafilomycin A1, which inhibits fusion of autophagosome and lysosome, and obtained similar results. Our findings indicate that the LC3-II accumulation induced by sorafenib results from activation of autophagosome formation but not from just inhibition of the autophagosome degradation steps. Second, we examined the color

change of mRFP-GFP tandem fluorescent-tagged LC3 (mRFP-GFP-LC3). When Huh7 cells were transfected with the mRFP-GFP-LC3 expression plasmid ptfLC3 and then treated with sorafenib, some punctate signals showed both GFP and mRFP signals but part of the punctate signals exhibited only mRFP signals (Fig. 2*b*). Because GFP fluorescence but not mRFP fluorescence is attenuated under lysosomal acidic condition,[13] this observation supports that autophagy induced by sorafenib proceeds to the lysosomal degradation phase. Finally, electron microscopy revealed abundant autophagic vacuoles such as autophagosomes and probably autolysosomes in sorafenib-treated Huh7 cells, but scarcely in control cells (Fig. 2*c*).

Sorafenib selectively inhibits the activity of TORC1 in hepatoma cells

Sorafenib was initially developed as a Raf kinase inhibitor, however, it can also inhibit other tyrosine kinases such as VEGR-2, Flt-3 and c-Kit.[17] The inhibitory effect of sorafenib on the Raf/MEK/ERK pathway[18] or the STAT3 pathway[19] is widely recognized in several types of cancer, but the effect of sorafenib on the PI3K/Akt pathway and the mTOR pathway has not been established yet. Because the mTOR pathway is known as a major regulatory pathway of autophagy,[20] we next examined the activity of the mTOR signaling pathway in Huh7 cells and HLF cells. Sorafenib clearly inhibited the activity of the mammalian target of rapamycin complex 1 (mTORC1), which is measured by the dephosphorylation of S6K and 4E-BP1 in Huh7 cells and HLF cells (Fig. 3*a*). 4E-BP1 is initially phosphorylated at threonine 37 and threonine 46, which promotes subsequent phosphorylation and decreases electrophoretic mobility.[21] With sorafenib administration, the upper band of phosphorylated 4E-BP1 gradually decreased and shifted to the lower band. At 24 hours after treatment initiation, the lower band diminished as well, indicating further dephosphorylation of 4E-BP1 at threonine 37 and 46. On the other hand, sorafenib treatment increased the phosphorylation of Akt at threonine 308 and serine 473 in these cells. The phosphorylation at threonine 308 suggests the activation of upstream PI3K while the phosphorylation at serine 473 suggests the activation of mTORC2.[22] Therefore, sorafenib can be presumed to possess a selective inhibitory effect on the activity of mTORC1 independent of PI3K and Akt. Administration of sorafenib clearly inhibited the phosphorylation of ERK as early as 2 hours after treatment, which is consistent with a previous report.[18] The expression of ATG7 and Beclin 1, autophagy-related gene products, did not change under sorafenib treatment. Next, we treated Huh7 cells with rapamycin or Torin1[23] to determine the impact of mTORC1 activity on autophagy induction. As expected, the levels of LC3-II increased upon rapamycin treatment in Huh7 cells (Fig. 3*b*). A similar result was obtained using another mTOR inhibitor, Torin1.

Inhibition of autophagy by siRNAs or a pharmacological inhibitor enhanced the apoptotic effect of sorafenib *in vitro*

From these results, we considered two possibilities: sorafenib-induced autophagy may be a mechanism of action of the antitumor effect of sorafenib or a stress-responsive phenomenon leading to survival of tumor cells in the presence of sorafenib treatment. To investigate the role of autophagy under sorafenib treatment, we introduced into Huh7 cells, the siRNA specific for *ATG7*. Administration of *ATG7* siRNA suppressed LC3-II expression in DMSO-treated cells and sorafenib-treated cells, indicating that autophagy is clearly suppressed under physiological conditions as well as with sorafenib treatment (Fig. 4*a*). Sorafenib treatment induced apoptosis, as determined by the elevation of caspase-3/7 activity or by the increase of Annexin V positive cells, and decreased the viability of Huh7 cells (Fig. 4*b*). Of importance is the finding that *ATG7* knockdown significantly enhanced the sorafenib-induced apoptosis and decreased cell viability in Huh7 cells. These observations imply that autophagy plays a protective role for hepatoma cells under sorafenib treatment and could be a target for enhancing its antitumor effects. We performed an ATG7 knockdown experiment using HLF cells as well and obtained a similar result (Fig. 4*c*).

Next, we treated Huh7 cells with sorafenib in combination with the pharmacological autophagy inhibitor chloroquine, which clearly blocks the downstream autophagic pathway in hepatoma cells as shown in Figure 2*a*. Chloroquine itself induced a modest activation of caspase-3/7 at a high dose under our experimental conditions (Fig. 5). However, in combination with sorafenib, chloroquine markedly enhanced the apoptotic effect of sorafenib and reduced cell viability in a dose-dependent manner. We investigated the effect of chloroquine on PLC/PRF/5 cells as well, and obtained a similar result.

Autophagy inhibitor chloroquine enhanced the anti-tumor effect of sorafenib in a xenograft model

To examine the significance of autophagy *in vivo*, nude mice were subcutaneously injected with Huh7 cells to generate xenograft tumors. To examine whether sorafenib induces autophagy in the *in vivo* setting, we administered sorafenib or vehicle for 7 days to mice bearing xenograft tumors. As we reported previously,[14] sorafenib treatment significantly suppressed tumor growth compared with the vehicle alone (data not shown). Consistent with the *in vitro* finding, xenograft tumors from sorafenib-administered mice displayed accumulation of LC3-II on immunoblot compared with those from vehicle-treated mice (Fig. 6*a*). To examine the therapeutic significance of autophagy inhibition for sorafenib therapy, mice with Huh7 xenograft were randomly assigned to two groups when the diameter of the subcutaneous tumor reached about 1 centimeter: sorafenib administration group and sorafenib plus chloroquine administration group. Coadministration of chloroquine and sorafenib for 7 days led to significant suppression of tumor growth compared with

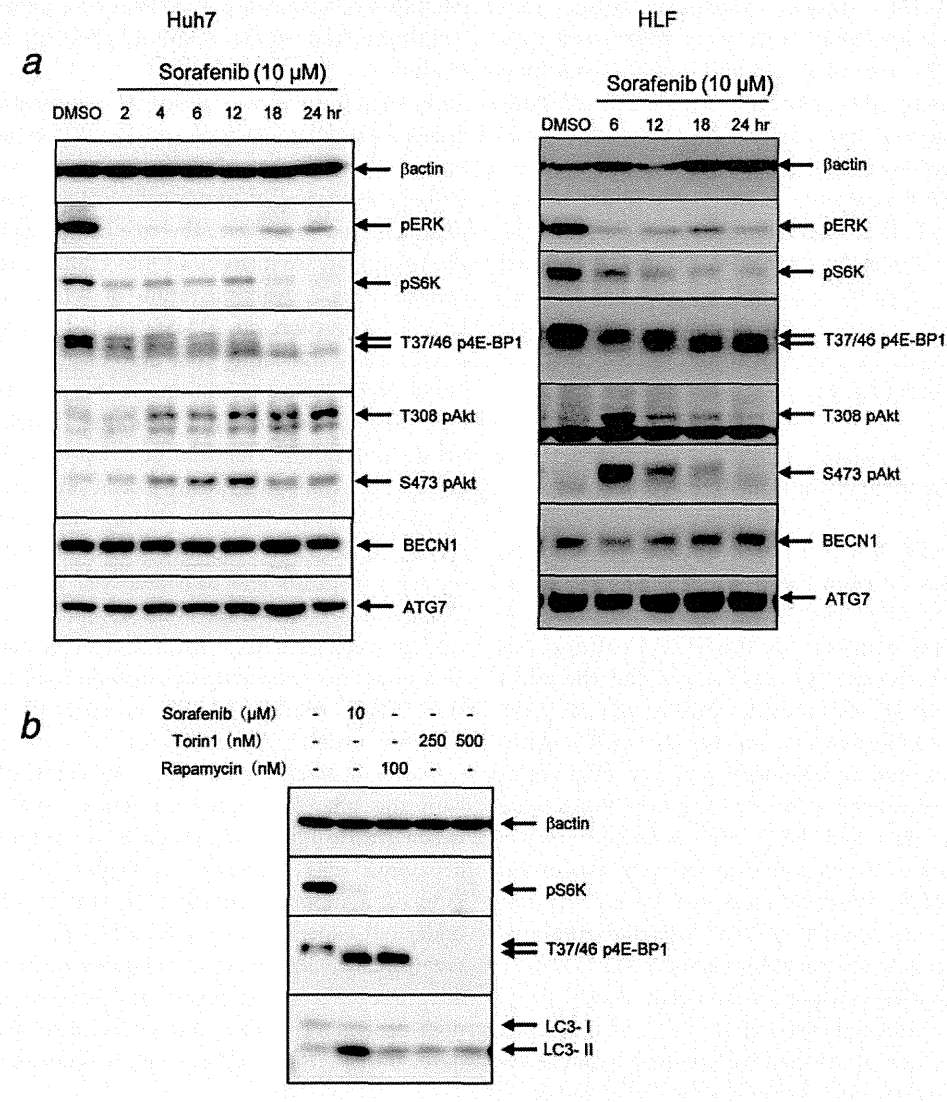

Figure 3. Raf/MEK/ERK and Akt/mTOR/S6K pathways in hepatoma cells treated with sorafenib. (*a*). Western blot showing decrease in ERK, S6K and 4E-BP1 phosphorylation, increase in Akt phosphorylation and stable expression of Beclin 1 and ATG7 in Huh7 cells and HLF cells after treatment with 10 μM sorafenib. (*b*). Western blot showing that rapamycin or Torin1 dephosphorylates both S6K and 4E-BP1 and increases the expression of LC3-II in Huh7 cells. Huh7 cells were treated with 100 nM rapamycin or the indicated concentration of Torin1 for 12 hr. Huh7 treated with sorafenib (10 μM, 12 hr) serves as a positive control. [Color figure can be viewed in the online issue, which is available at wileyonlinelibrary.com.]

administration of sorafenib alone (Fig. 6*b*). Administration of chloroquine alone did not affect the growth of the tumor. We performed TUNEL staining and immunohistological staining of cleaved caspase-3 of the xenograft tumor to examine the contribution of apoptosis in this xenograft model. However, nonspecific staining of the xenograft tumors treated with sorafenib interfered with an accurate evaluation of the apoptotic change (data not shown).

Discussion

Accumulating evidence indicates that cancer therapies such as irradiation and administration of cytotoxic drugs and chemicals induce autophagy and autophagic cell death in a variety of tumor cells.[8] Research has shown that autophagy induced by these treatments sometimes protects tumor cells (autophagic resistance) but promotes cell death in other settings (autophagic Type II programmed cell death). For example, temozolomide, a DNA alkylating agent,[24] and ionizing radiation[25] induce autophagy in malignant glioma cells and a variety of epithelial tumors, respectively, and this inhibition enhances antitumor effects. On the other hand, poly(dI:dC) induces endosome-mediated autophagy leading to cell death in melanoma cells.[26] Arsenic trioxide induces autophagic cell death in leukemia cells.[27] In the present study, we demonstrated that sorafenib, a recently approved molecular targeting drug for HCC, induced autophagy which appeared to

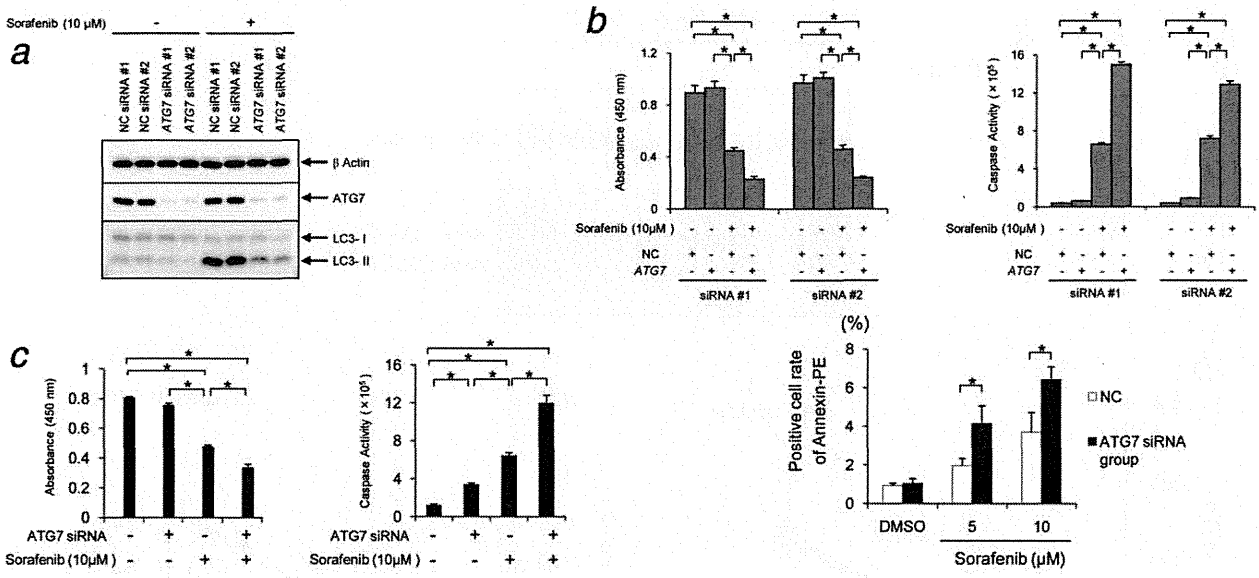

Figure 4. Genetic ablation of autophagy increases sensitivity of hepatoma cells to sorafenib. (*a*,*b*). Huh7 cells were transfected with two different sets of *ATG7* siRNA (no. 1 and 2) or control siRNA (no. 1 and 2) for 48 hr and then treated with the indicated concentration of sorafenib or vehicle for an additional 18 hr. LC3 lipidation and ATG7 expression were determined by western blot (*a*). Cell growth was determined by WST assay, while apoptosis was monitored by the activity of caspase-3/7 in the supernatant or by annexin V positive cell rate ($n = 4$) (*b*). (*c*) HLF cells were transfected with *ATG7* siRNA and examined for cell viability and caspase-3/7 activity in the same manner as Huh7 cells ($n = 4$). *$p < 0.05$. [Color figure can be viewed in the online issue, which is available at wileyonlinelibrary.com.]

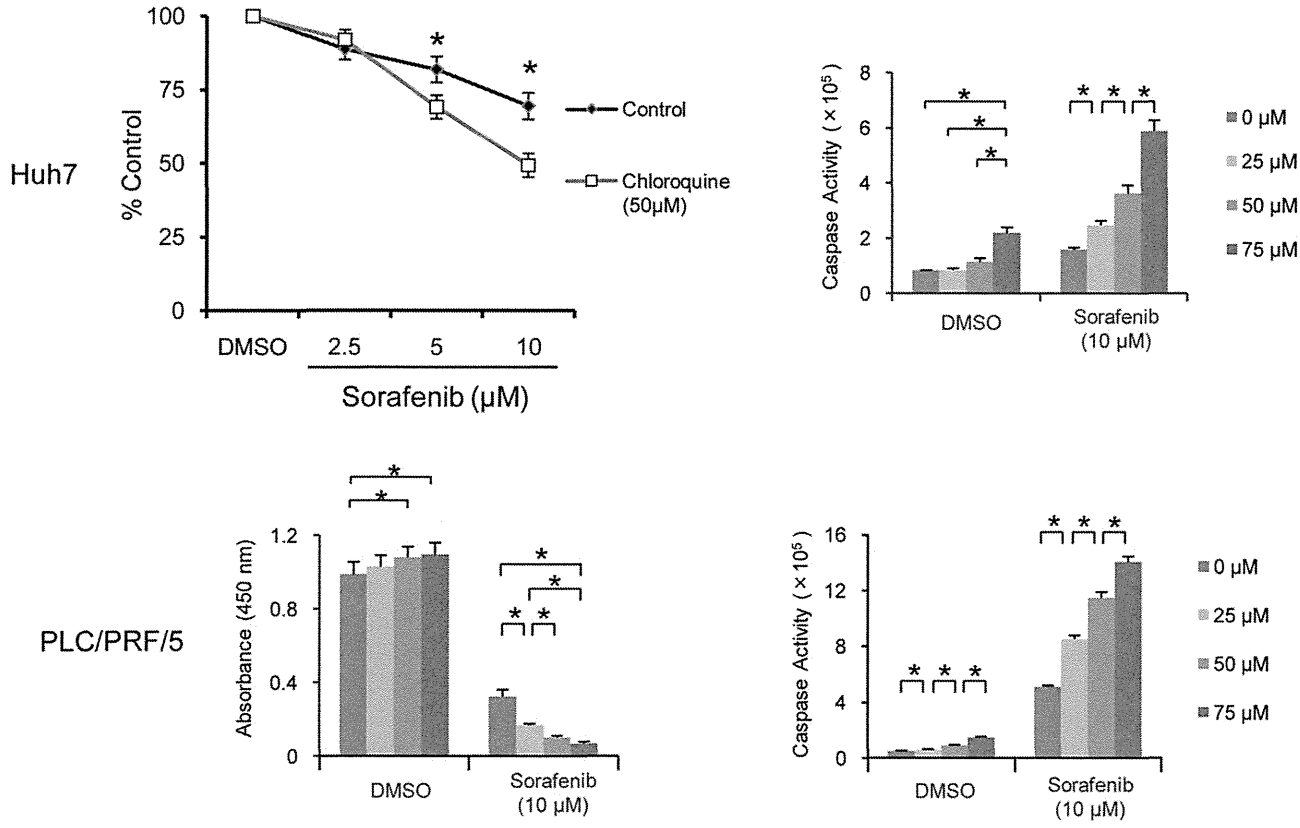

Figure 5. Pharmacological inhibition of autophagy increases sensitivity of hepatoma cells to sorafenib. Huh7 cells or PLC/PRF/5 cells were treated with or without the indicated concentration of sorafenib in the presence or absence of chloroquine for 18 hr. Capsase-3/7 activity was monitored in the supernatant, while cell growth was determined by WST assay ($n = 4$). *$p < 0.05$.

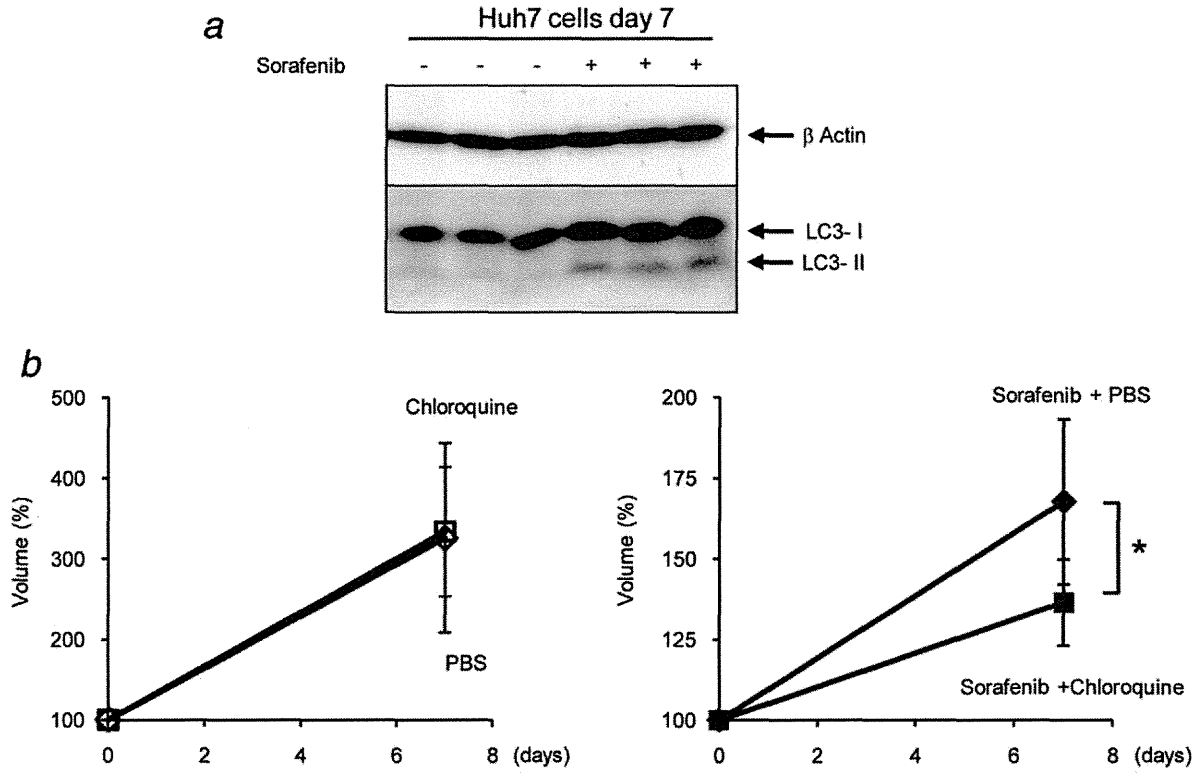

Figure 6. Inhibition of autophagy potentiates sorafenib-induced antitumor effects in Huh7 xenograft. (*a*). Western blot showing increase in LC3-II expression in Huh7 xenograft tumor after sorafenib therapy. Mice bearing xenograft tumor were administered sorafenib (30 mg kg^{-1}) or vehicle for 7 days ($n = 3$/group). (*b*). Chloroquine (60 mg kg^{-1}) itself did not affect the tumor growth of Huh7 xenograft (left panel), ($n = 7$/group), but enhanced the effect of sorafenib (30 mg kg^{-1}) in a synergistic manner (right panel), ($n = 6$/group). Mice bearing xenograft tumor were administered sorafenib and/or chloroquine for 7 days. Tumor volume at 7 days is shown as a percentage of that before initiation of the therapy. *$p < 0.05$. [Color figure can be viewed in the online issue, which is available at wileyonlinelibrary.com.]

promote survival of hepatoma cells and thereby may be a cellular adaptive response related to primary resistance to this compound.

LC3 lipidation and its association with the isolation membranes have been established as useful signs for autophagy detectable by immunoblotting and fluorescence microscopy, facilitating research on autophagy. Previous research has shown that sorafenib induces GFP-LC3 punctate structure and LC3-II conversion in tumor cells.[9–11] However, these techniques should be analyzed more carefully, because positive results clearly indicate increased numbers of autophagosomes but do not always mean upregulation of autophagic flux.[28] For example, treatment with vinblastine or nocodazole leads to LC3 conversion and produces GFP-LC3 punctate structures, resulting from blockade of the fusion of autophagosomes and lysosomes but not from autophagy induction.[29,30] In the present study, we applied several methods including LC3 turnover assay using a lysosomal inhibitor of chloroquine or bafilomycin A1, measurement of the amount of a selective autophagy substrate p62, and observation of the mRFP-GFP color change using a fluorescent-tagged LC3 probe, to obtain evidence showing that sorafenib not only increases the number of autophagosomes but also activates the autophagic flux.

The underlying mechanisms by which sorafenib induces autophagy are not completely clear at present. In addition to the well-known target Raf/MEK/MAPK pathway, sorafenib clearly inhibited the mTORC1 pathway in the present study. Because mTOR inhibition by rapamycin or Torin1 activates autophagosome formation in hepatoma cells, sorafenib-induced inhibition of the mTORC1 pathway might be involved in sorafenib-mediated induction of autophagy. Recently, a putative tumor-suppressor gene *p53* has been shown to transactivate an autophagy-inducing gene, *dram*,[31] and *p53*-dependent induction of autophagy has been documented in response to DNA damage or reexpression of p53 in p53-negative tumor cells.[32] Because the hepatoma cells used in the present study (Huh7, HLF and PLC/PRF/5) possess mutant *p53*, sorafenib-induced adaptive autophagy could occur independently of p53. This finding may be important, because more than half of advanced HCC cases are p53-defective.[33] In such cases, our observations could be applicable and relevant.

Study of rodent carcinogenesis has revealed that autophagic protein degradation is reduced in HCC.[34] In human,

malignant HCC cell lines and HCC tissue with recurrent disease display lower autophagic activity with decreased expression of Beclin 1.[35] The autophagic pathway contributes to the growth-inhibitory effect of TGF-beta in hepatoma cells.[36] Taken together, these findings suggest that defects in autophagy may promote development or progression of HCC, focusing on the tumor suppressive or antitumor effect of autophagy in the liver or HCC. In contrast, the present study clearly showed that autophagy induced by sorafenib protects hepatoma cells from apoptotic cell death, thus shedding light on the tumor-promoting effect of autophagy in HCC. Inhibition of autophagy at both an early step (by *ATG7* knockdown) and a late step (by chloroquine treatment) sensitized hepatoma cells by converting the autophagic process to an apoptotic process. Of importance are the findings that sorafenib induced autophagy in a xenograft model and that coadministration of chloroquine and sorafenib led to better suppression of xenograft tumor than sorafenib alone. Although further study is needed to elucidate the mechanism(s) involved in autophagy-mediated protection of tumor cells, the induced autophagy might degrade the damaged or harmful cellular proteins and organelles to suppress apoptosis and promote survival of hepatoma cells under sorafenib treatment.

In conclusion, the present study demonstrates both *in vitro* and *in vivo* that sorafenib induces autophagosome formation and upregulates cellular autophagy in tumor cells, which is an adaptive response to this drug, and raises the important possibility that autophagy may be a novel target for cancer treatment with sorafenib therapy.

Acknowledgements

The authors thank David Sabatini's laboratory (Whitehead Institute for Biomedical Research) and Nathanael Gray's laboratory (Dana-Farber Cancer Institute) for providing Torin1. They also thank Bayer HealthCare Pharmaceuticals Inc. (Wayne, NJ) for providing sorafenib.

References

1. Finn RS. Drug therapy: sorafenib. *Hepatology* 2010;51:1843–9.
2. Llovet JM, Ricci S, Mazzaferro V, Hilgard P, Gane E, Blanc JF, de Oliveira AC, Santoro A, Raoul JL, Forner A, Schwartz M, Porta C, et al. Sorafenib in advanced hepatocellular carcinoma. *N Engl J Med* 2008;359:378–90.
3. Cheng AL, Kang YK, Chen Z, Tsao CJ, Qin S, Kim JS, Luo R, Feng J, Ye S, Yang TS, Xu J, Sun Y, et al. Efficacy and safety of sorafenib in patients in the Asia-Pacific region with advanced hepatocellular carcinoma: a phase III randomised, double-blind, placebo-controlled trial. *Lancet Oncol* 2009;10:25–34.
4. Yoshimori T. Autophagy: a regulated bulk degradation process inside cells. *Biochem Biophys Res Commun* 2004;313:453–8.
5. Tsujimoto Y, Shimizu S. Another way to die: autophagic programmed cell death. *Cell Death Differ* 2005;12 (Suppl 2):1528–34.
6. White E, DiPaola RS. The double-edged sword of autophagy modulation in cancer. *Clin Cancer Res* 2009;15:5308–16.
7. Qu X, Yu J, Bhagat G, Furuya N, Hibshoosh H, Troxel A, Rosen J, Eskelinen EL, Mizushima N, Ohsumi Y, Cattoretti G, Levine B. Promotion of tumorigenesis by heterozygous disruption of the beclin 1 autophagy gene. *J Clin Invest* 2003;112: 1809–20.
8. Kondo Y, Kanzawa T, Sawaya R, Kondo S. The role of autophagy in cancer development and response to therapy. *Nat Rev Cancer* 2005;5: 726–34.
9. Ullén A, Farnebo M, Thyrell L, Mahmoudi S, Kharaziha P, Lennartsson L, Grandér D, Panaretakis T, Nilsson S. Sorafenib induces apoptosis and autophagy in prostate cancer cells in vitro. *Int J Oncol* 2010;37:15–20.
10. Park MA, Zhang G, Martin AP, Hamed H, Mitchell C, Hylemon PB, Graf M, Rahmani M, Ryan K, Liu X, Spiegel S, Norris J, et al. Vorinostat and sorafenib increase ER stress, autophagy and apoptosis via ceramide-dependent CD95 and PERK activation. *Cancer Biol Ther* 2008;7:1648–62.
11. Park MA, Reinehr R, Häussinger D, Voelkel-Johnson C, Ogretmen B, Yacoub A, Grant S, Dent P. Sorafenib activates CD95 and promotes autophagy and cell death via Src family kinases in gastrointestinal tumor cells. *Mol Cancer Ther* 2010;9:2220–31.
12. Shimizu S, Takehara T, Hikita H, Kodama T, Miyagi T, Hosui A, Tatsumi T, Ishida H, Noda T, Nagano H, Doki Y, Mori M, et al. The let-7 family of microRNAs inhibits Bcl-xL expression and potentiates sorafenib-induced apoptosis in human hepatocellular carcinoma. *J Hepatol* 2010; 52:698–704.
13. Kimura S, Noda T, Yoshimori T. Dissection of the autophagosome maturation process by a novel reporter protein, tandem fluorescent-tagged LC3. *Autophagy* 2007;3:452–60.
14. Hikita H, Takehara T, Shimizu S, Kodama T, Shigekawa M, Iwase K, Hosui A, Miyagi T, Tatsumi T, Ishida H, Li W, Kanto T, et al. The Bcl-xL inhibitor, ABT-737, efficiently induces apoptosis and suppresses growth of hepatoma cells in combination with sorafenib. *Hepatology* 2010;52:1310–21.
15. Mizushima N, Yoshimori T. How to interpret LC3 immunoblotting. *Autophagy* 2007;3:542–5.
16. Bjørkøy G, Lamark T, Brech A, Outzen H, Perander M, Overvatn A, Stenmark H, Johansen T. p62/SQSTM1 forms protein aggregates degraded by autophagy and has a protective effect on huntingtin-induced cell death. *J Cell Biol* 2005;171:603–14.
17. Sridhar SS, Hedley D, Siu LL. Raf kinase as a target for anticancer therapeutics. *Mol Cancer Ther* 2005;4:677–85.
18. Liu L, Cao Y, Chen C, Zhang X, McNabola A, Wilkie D, Wilhelm S, Lynch M, Carter C. Sorafenib blocks the RAF/MEK/ERK pathway, inhibits tumor angiogenesis, and induces tumor cell apoptosis in hepatocellular carcinoma model PLC/PRF/5. *Cancer Res* 2006;66:11851–8.
19. Blechacz BR, Smoot RL, Bronk SF, Werneburg NW, Sirica AE, Gores GJ. Sorafenib inhibits signal transducer and activator of transcription-3 signaling in cholangiocarcinoma cells by activating the phosphatase shatterproof 2. *Hepatology* 2009;50:1861–70.
20. Díaz-Troya S, Pérez-Pérez ME, Florencio FJ, Crespo JL. The role of TOR in autophagy regulation from yeast to plants and mammals. *Autophagy* 2008;4:851–65.
21. Gingras AC, Gygi SP, Raught B, Polakiewicz RD, Abraham RT, Hoekstra MF, Aebersold R, Sonenberg N. Regulation of 4E-BP1 phosphorylation: a novel two-step mechanism. *Genes Dev* 1999;13:1422–37.
22. Foster KG, Fingar DC. Mammalian target of rapamycin (mTOR): conducting the cellular signaling symphony. *J Biol Chem* 2010;285: 14071–7.
23. Thoreen CC, Kang SA, Chang JW, Liu Q, Zhang J, Gao Y, Reichling LJ, Sim T, Sabatini DM, Gray NS. An ATP-competitive mammalian target of rapamycin inhibitor reveals rapamycin-resistant functions of mTORC1. *J Biol Chem* 2009;284: 8023–32.
24. Kanzawa T, Germano IM, Komata T, Ito H, Kondo Y, Kondo S. Role of autophagy in temozolomide-induced cytotoxicity for malignant glioma cells. *Cell Death Differ* 2004;11:448–57.
25. Paglin S, Hollister T, Delohery T, Hackett N, McMahill M, Sphicas E, Domingo D, Yahalom J. A novel response of cancer cells to radiation involves autophagy and formation of acidic vesicles. *Cancer Res* 2001;61:439–44.
26. Tormo D, Checińska A, Alonso-Curbelo D, Pérez-Guijarro E, Cañón E, Riveiro-Falkenbach E, Calvo TG, Larribere L, Megías D, Mulero F, Piris

MA, Dash R, et al. Targeted activation of innate immunity for therapeutic induction of autophagy and apoptosis in melanoma cells. *Cancer Cell* 2009;16:103–14.
27. Goussetis DJ, Altman JK, Glaser H, McNeer JL, Tallman MS, Platanias LC. Autophagy is a critical mechanism for the induction of the antileukemic effects of arsenic trioxide. *J Biol Chem* 2010;285: 29989–97.
28. Mizushima N, Yoshimori T, Levine B. Methods in mammalian autophagy research. *Cell* 2010;140: 313–26.
29. Seglen PO, Brinchmann MF. Purification of autophagosomes from rat hepatocytes. *Autophagy* 2010;6:542–7.
30. Bampton ET, Goemans CG, Niranjan D, Mizushima N, Tolkovsky AM. The dynamics of autophagy visualized in live cells: from autophagosome formation to fusion with endo/lysosomes. *Autophagy* 2005;1:23–36.
31. Crighton D, Wilkinson S, O'Prey J, Syed N, Smith P, Harrison PR, Gasco M, Garrone O, Crook T, Ryan KM. DRAM, a p53-induced modulator of autophagy, is critical for apoptosis. *Cell* 2006;126:121–34.
32. Amaravadi RK, Yu D, Lum JJ, Bui T, Christophorou MA, Evan GI, Thomas-Tikhonenko A, Thompson CB. Autophagy inhibition enhances therapy-induced apoptosis in a Myc-induced model of lymphoma. *J Clin Invest* 2007;117:326–36.
33. Hussain SP, Schwank J, Staib F, Wang XW, Harris CC. TP53 mutations and hepatocellular carcinoma: insights into the etiology and pathogenesis of liver cancer. *Oncogene* 2007;26: 2166–76.
34. Kisen GO, Tessitore L, Costelli P, Gordon PB, Schwarze PE, Baccino FM, Seglen PO. Reduced autophagic activity in primary rat hepatocellular carcinoma and ascites hepatoma cells. *Carcinogenesis* 1993;14: 2501–5.
35. Ding ZB, Shi YH, Zhou J, Qiu SJ, Xu Y, Dai Z, Shi GM, Wang XY, Ke AW, Wu B, Fan J. Association of autophagy defect with a malignant phenotype and poor prognosis of hepatocellular carcinoma. *Cancer Res* 2008;68: 9167–75.
36. Kiyono K, Suzuki HI, Matsuyama H, Morishita Y, Komuro A, Kano MR, Sugimoto K, Miyazono K. Autophagy is activated by TGF-beta and potentiates TGF-beta-mediated growth inhibition in human hepatocellular carcinoma cells. *Cancer Res* 2009;69:8844–52.

Research Article

EASL EUROPEAN ASSOCIATION FOR THE STUDY OF THE LIVER | JOURNAL OF HEPATOLOGY

Bak deficiency inhibits liver carcinogenesis: A causal link between apoptosis and carcinogenesis

Hayato Hikita[1], Takahiro Kodama[1], Satoshi Shimizu[1], Wei Li[1], Minoru Shigekawa[1], Satoshi Tanaka[1], Atsushi Hosui[1], Takuya Miyagi[1], Tomohide Tatsumi[1], Tatsuya Kanto[1], Naoki Hiramatsu[1], Eiichi Morii[2], Norio Hayashi[3], Tetsuo Takehara[1,*]

[1]*Department of Gastroenterology and Hepatology, Osaka University Graduate School of Medicine, Suita, Osaka 565-0871, Japan;*
[2]*Department of Pathology, Osaka University Graduate School of Medicine, Suita, Osaka 565-0871, Japan;*
[3]*Kansai-Rosai Hospital, Amagasaki, Hyogo 660-8511, Japan*

Background & Aims: Hepatocyte apoptosis is a key feature of chronic liver disease including viral hepatitis and steatohepatitis. A previous study demonstrated that absence of the Bcl-2 family protein Mcl-1 led to increased hepatocyte apoptosis and development of liver tumors in mice. Since Mcl-1 not only inhibits the mitochondrial pathway of apoptosis but can also inhibit cell cycle progression and promote DNA repair, it remains to be proven whether the tumor suppressive effects of Mcl-1 are mediated by prevention of apoptosis.

Methods: We examined liver tumor development, fibrogenesis, and oxidative stress in livers of hepatocyte-specific knockout (KO) of *Mcl-1* or *Bcl-xL*, another key antagonist of apoptosis in hepatocytes. We also examined the impact of additional KO of *Bak*, a downstream molecule of Mcl-1 towards apoptosis but not the cell cycle or DNA damage pathway, on tumor development, hepatocyte apoptosis, and inflammation.

Results: *Bcl-xL* KO led to a high incidence of liver tumors in 1.5-year-old mice, similar to *Mcl-1* KO. Bcl-xL- or Mcl-1-deficient livers showed higher levels of TNF-α production and oxidative stress than wild-type livers at as early as 6 weeks of age and oxidative DNA damage at 1.5 years. Deletion of Bak significantly inhibited hepatocyte apoptosis in *Mcl-1* KO mice and reduced the incidence of liver cancer, coinciding with reduction of TNF-α production, oxidative stress, and oxidative DNA damage in non-cancerous livers.

Conclusions: Our findings strongly suggest that chronically increased apoptosis in hepatocytes is carcinogenic and offer genetic evidence that inhibition of apoptosis may suppress liver carcinogenesis in chronic liver disease.

Keywords: Bcl-xL; Mcl-1; 8-OHdG.
Received 26 September 2011; received in revised form 19 January 2012; accepted 21 January 2012; available online 10 March 2012
* Corresponding author. Address: Department of Gastroenterology and Hepatology, Osaka University Graduate School of Medicine, 2-2 Yamada-oka, Suita, Osaka 565-0871, Japan. Tel.: +81 6 6879 3621; fax: +81 6 6879 3629.
E-mail address: takehara@gh.med.osaka-u.ac.jp (T. Takehara).
Abbreviations: HCC, hepatocellular carcinoma; ALT, alanine aminotransferase; RT-PCR, reverse-transcription PCR; HO-1, heme oxygenase-1; NQO1, NAD(P)H:quinone oxidoreductase 1; 8-OHdG, 8-hydroxy-2′-deoxyguanosine; TUNEL, terminal deoxynucleotidyl transferase-mediated deoxyuridine triphosphate nick-end labeling.

Introduction

Apoptosis of epithelial cells, as well as infiltration of inflammatory cells or deposits of fibers, is frequently observed in the chronic diseased liver, which is a high-risk condition for hepatocellular carcinoma (HCC) [1]. For example, Fas-mediated hepatocyte apoptosis is a mechanism of cell death in chronic hepatitis C virus infection and hepatitis B virus infection [2,3]. Hepatocyte apoptosis shows correlation with inflammation and fibrosis in non-alcoholic steatohepatitis [4]. Cytokeratin 18 neoepitope, a well-established marker of caspase activity in serum, is elevated and associated with liver injury in chronic viral hepatitis and non-alcoholic steatohepatitis [5–7]. Although viral factors and overt organ inflammation linked to liver cancer development have been extensively studied [8,9], less information is available on the involvement of hepatocyte apoptosis in liver cancer development.

Bcl-xL and Mcl-1 are among the anti-apoptotic members of the Bcl-2 family, which antagonizes the pro-apoptotic function of Bak and/or Bax at the mitochondrial outer membrane. We previously reported that hepatocyte-specific *Bcl-xL* or *Mcl-1* knockout (KO) mice showed persistent apoptosis of hepatocytes in the adult liver and mild fibrotic responses [10,11]. A very recent study by Weber *et al.* [12] demonstrated that hepatocyte-specific *Mcl-1* KO mice developed liver tumors in old age. This observation raised the important possibility that apoptosis in hepatocytes could lead to the development of liver cancer. However, as Mcl-1 has been reported to possess functions other than anti-apoptosis, such as cell cycle inhibition [13,14] and DNA damage repair [15,16], it is difficult to conclude that the phenotypes observed in *Mcl-1* KO are simply ascribable to apoptosis. Indeed, *Mcl-1* KO mice showed not only increased apoptosis but also increased regeneration in the liver [12]. In the present study, we demonstrated that hepatocyte-specific *Bcl-xL* KO mice also develop liver cancer in old age and that deficiency of Bak, a downstream effector molecule of Mcl-1 towards the

Table 1. Incidence of liver tumors in KO mice.

Age (yr)	Genotype	Tumor incidence
1.5		
	Bcl-xL$^{+/+}$	0% (0/10)
	Bcl-xL$^{-/-}$	88% (7/8)*
1		
	Bcl-xL$^{+/+}$	0% (0/4)
	Bcl-xL$^{-/-}$	27% (3/11)
1.5		
	Mcl-1$^{+/+}$	0% (0/22)
	Mcl-1$^{-/-}$	100% (16/16)*
1		
	Mcl-1$^{-/-}$ *Bak*$^{+/+}$	64% (14/22)
	Mcl-1$^{-/-}$ *Bak*$^{-/-}$	0% (0/7)*

*p <0.05 *vs.* control.

mitochondrial pathway of apoptosis, clearly suppresses hepatocyte apoptosis and liver carcinogenesis in *Mcl-1* KO mice. We also considered possible mechanisms involving oxidative stress that underlie elevated malignant transformation in the apoptosis-prone liver. The present study offers strong support for the hypothesis that chronically increased apoptosis in hepatocytes is carcinogenic. It also provides genetic evidence that inhibition of apoptosis may suppress liver carcinogenesis in chronic liver disease.

Materials and methods

Mice

Conditional *Bcl-xL* KO mice (*bcl-x*^{floxflox} *Alb-Cre*) and *Mcl-1* KO mice (*mcl-1*^{floxflox} *Alb-Cre*) were previously described [11]. We purchased *Bak* KO mice (*bak*$^{-/-}$) from the Jackson Laboratory (Bar Harbor, ME). We generated hepatocyte-specific Bak/Mcl-1 double KO mice (*bak*$^{-/-}$ *mcl-1*^{floxflox} *Alb-Cre*) by mating the strains. They were maintained in a specific pathogen-free facility and treated with humane care with approval from the Animal Care and Use Committee of Osaka University Medical School. Measurement of serum alanine aminotransferase (ALT) level, caspase-3/7 activity and histological analyses have been previously described [11].

Western blot analysis

For immunodetection, the following antibodies were used: anti-Bcl-xL antibody (Santa Cruz Biotechnology, Santa Cruz, CA), anti-Mcl-1 antibody (Rockland, Gilbertsville, PA), anti-Bak antibody (Millipore, Billerica, MA), anti-Bax antibody, anti-ERK antibody, anti-phospho-ERK antibody, anti-p38 antibody, anti-phospho-p38 antibody, anti-JNK antibody, anti-phospho-JNK antibody, anti-PCNA antibody (Cell Signaling Technology, Danvers, MA), and anti-beta-actin antibody (Sigma-Aldrich, Saint Louis, MO).

Real-time reverse-transcription PCR (RT-PCR)

The following TaqMan Gene Expression Assays (Applied Biosystems, Foster City, CA) were used: mouse-AFP (Mm00431715_m1), mouse-glypican-3 (Mm00516722_m1), mouse-IL-6 (Mm00446190_m1), mouse-TNF-α (Mm00443258_m1), mouse-MCP-1 (Mm00441242_m1), mouse-CD68 (Mm03047343_m1), mouse-CD4 (Mm00442754_m1), mouse-CD8 (Mm01182108_m1), mouse-heme oxygenase-1 (HO-1) (Mm00516005_m1), mouse-NAD(P)H:quinone oxidoreductase 1 (NQO1) (Mm00500821_m1), and mouse-Beta actin (Mm00607939_s1). All expression levels were corrected with the quantified expression level of beta actin.

Immunohistochemistry

8-Hydroxy-2′-deoxyguanosine (8-OHdG), cleaved caspase-9, PCNA, and ki-67 were labeled in paraffin-embedded liver sections using anti-8-OHdG antibody (Nikken Seil, Tokyo, Japan), anti-cleaved caspase-9 antibody, anti-PCNA antibody (Cell Signaling Technology), and anti-ki-67 antibody (Dako, Tokyo, Japan), respectively. Terminal deoxynucleotidyl transferase-mediated deoxyuridine triphosphate nick-end labeling (TUNEL) was performed according to a previously reported procedure [17].

Statistical analysis

Data are presented as mean ± SD. Differences between two groups were determined using the Student's *t*-test for unpaired observations. Carcinogenesis rates were analyzed using the Chi-square test. Multiple comparisons of *Bak/Mcl-1* double KO mice were performed by ANOVA followed by Scheffe *post hoc* correction. Fisher *post hoc* correction was used for the other multiple comparisons. A p <0.05 was considered statistically significant.

Results

Bcl-xL KO mice develop liver tumors in old age

We previously reported that hepatocyte-specific *Bcl-xL* KO mice developed spontaneous hepatocyte apoptosis by the mitochondrial pathway (Supplementary Fig. 1A) at as early as 1 month of age with a gradual increase in the liver fibrotic response from 3 to 7 months [10]. To examine the phenotypes at later time points, we sacrificed *Bcl-xL* KO mice and their control littermates at 1 and 1.5 years of age. Macroscopic tumors had developed in the liver of 27% and 88% of the KO mice, respectively, but not in the control littermates (Fig. 1A and Table 1). Most of the *Bcl-xL* KO mice had multiple tumors and the liver body-weight ratio for *Bcl-xL* KO mice was significantly higher than that of the control mice (Fig. 1B and C). Tumors were histologically defined as well-differentiated HCCs (Fig. 1D). To find out whether the *bcl-x* gene is really targeted in the tumors, we performed Western blot analysis for the expression of the Bcl-2 family proteins (Fig. 1E and Supplementary Fig. 2A). The tumors were confirmed to be deficient for Bcl-xL, excluding the possibility that transformed cells arising from hepatocytes in which the *bcl-x* gene was not deleted had expanded to form tumors. Interestingly, most of these tumors showed apparently higher levels of Mcl-1 expression than the wild-type liver or the non-cancerous surrounding tissues. Reciprocal overexpression of Mcl-1 may explain the possible survival advantage of these tumors. Tumors in *Bcl-xL* KO mice expressed higher levels of α-fetoprotein (Fig. 1F) and frequently showed activation of ERK and JNK (Fig. 1G), which are observed in human HCC [18,19].

Liver tumors in Mcl-1 KO mice show similar characteristics to human HCC

We have previously reported phenotypes of hepatocyte-specific *Mcl-1* KO mice, which display spontaneous hepatocyte apoptosis by the mitochondrial pathway (Supplementary Fig. 1B) and liver fibrotic responses at an early age [11]. Since our *Mcl-1* floxed mice differed from those of Weber *et al.* [12] in origin, we next examined the development of liver tumors in our hepatocyte-specific *Mcl-1* KO mice. All the *Mcl-1* KO mice, but none of the control littermates, developed liver tumors at 1.5 years of age, with a significant increase of liver body-weight ratio (Fig. 2A–C

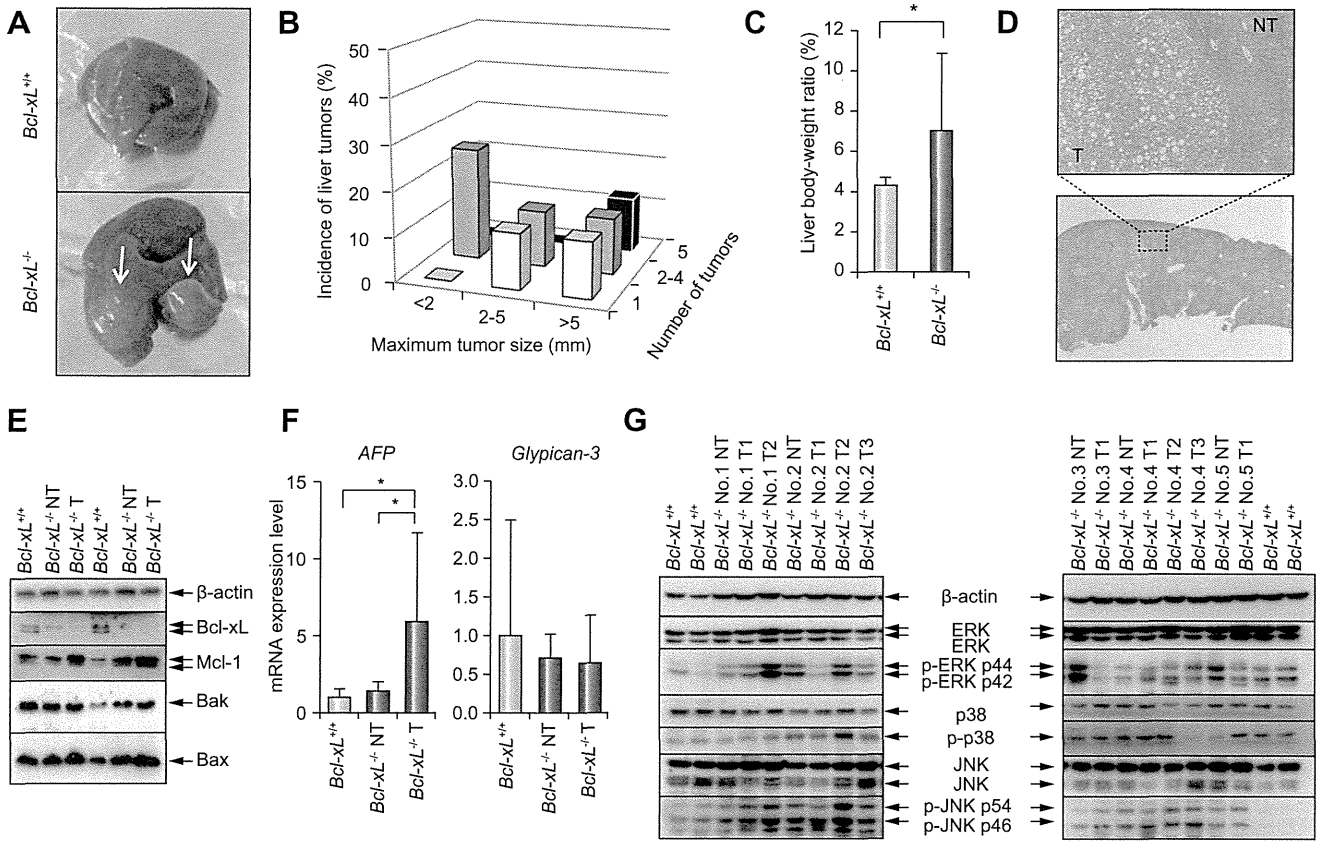

Fig. 1. Liver tumors in *Bcl-xL* KO mice. (A–E) Hepatocyte-specific *Bcl-xL*-deficient mice (*Bcl-xL*$^{-/-}$) (N = 8) and their control littermates (*Bcl-xL*$^{+/+}$) (N = 10) were sacrificed at 1.5 years of age. (A) Representative macroscopic view of the livers with arrows indicating tumors. (B) Incidence of liver tumors separated by maximum tumor size and number of tumors. (C) Liver body-weight ratio. (D) Representative histology of liver tumors in *Bcl-xL* KO mice. (E) Western blot of the Bcl-2 family proteins in tumors (T) and surrounding non-cancerous livers (NT) of *Bcl-xL* KO mice and livers of control mice. (F and G) Characteristics of liver tumors in *Bcl-xL* KO mice. (F) Real-time RT-PCR analysis of the expression levels of α-fetoprotein (*AFP*) and *glypican-3* mRNA (N = 9 or 10 per group). (G) Expression and activation of mitogen-activated protein kinases. *p <0.05.

and Table 1). As in the case of tumors of *Bcl-xL* KO mice, liver tumors that developed in *Mcl-1* KO mice were deficient for Mcl-1 expression and, in most cases, reciprocally overexpressed Bcl-xL (Fig. 2E and Supplementary Fig. 2B). These tumors expressed higher levels of α-fetoprotein and glypican-3 (Fig. 2F) and frequently showed activation of ERK and JNK (Fig. 2G).

Inflammatory response and oxidative stress occur in Bcl-xL- or Mcl-1-KO livers

To examine the molecular mechanism of tumor development, we examined gene expression in the livers of 6-week-old *Bcl-xL* or *Mcl-1* KO mice. Real-time RT-PCR analysis revealed increases of inflammatory cytokine TNF-α, but not IL-6, and chemokine MCP-1 in *Bcl-xL* and *Mcl-1* KO livers (Fig. 3A and B), despite overt histological inflammation (data not shown). Together with an increase of MCP-1, CD68 expression was significantly higher in KO livers than in control livers (Fig. 3C and D). In contrast, there was no difference in the expression of CD4 and CD8 between the groups. These findings suggest that activation or infiltration of myeloid-derived cells and production of TNF-α are characteristic of the *Bcl-xL* or *Mcl-1* KO liver. Together with the previous study reporting that TNF-α promotes cellular transformation [20], these results suggest that the increase in TNF-α may be one of the mechanisms of tumor development.

Since oxidative stress is also reported to cause carcinogenesis [21], we examined the expression of HO-1 and NQO1, inducible anti-oxidant enzymes, and 8-OHdG in the liver tissues. Real-time RT-PCR analysis revealed that HO-1 and NQO-1 expressions were significantly increased in *Mcl-1* KO livers at 6 weeks (Fig. 3E). 8-OHdG staining revealed that there were few 8-OHdG positive nuclei in both *Mcl-1* KO and the control liver at 6 weeks of age. However, scattered positive nuclei were observed in KO livers at 1.5 years of age, but not in the tumors, and the number of positive nuclei was significantly higher in KO livers than in control livers (Fig. 3F and Supplementary Fig. 3). Similarly, the number of 8-OHdG positive nuclei was significantly higher in *Bcl-xL* KO livers at 1.5 years of age than in control livers (Fig. 3G). These results suggest that oxidative stress may occur at as early as 6 weeks of age in KO livers and that oxidative injury arises at a later time point.

Bak deficiency significantly ameliorates hepatocyte apoptosis and reduces tumor development in Mcl-1 KO mice

Bak is a proapoptotic Bcl-2 family protein, which is able to oligmerize to form pores at the outer membrane of mitochondria. To understand whether inhibition of apoptosis could reduce the carcinogenic potential, we crossed *Mcl-1* KO mice and *Bak* KO mice and generated *Bak Mcl-1* double KO mice. As expected, *Bak* KO significantly suppressed hepatocyte apoptosis in *Mcl-1*